Acoustic response of submarine volcanoes in the Tofua Arc and northern Lau Basin to two great earthquakes

Citation	Bohnenstiehl, D. R., Dziak, R. P., Matsumoto, H., & Conder, J. A. (2013). Acoustic response of submarine volcanoes in the Tofua Arc and northern Lau Basin to two great earthquakes. Geophysical Journal International, 196(3), 1657-1675. doi:10.1093/gji/ggt472
DOI	10.1093/gji/ggt472
Publisher	Oxford University Press
Version	Version of Record
Citable Link	http://hdl.handle.net/1957/46933
Terms of Use	http://cdss.library.oregonstate.edu/sa-termsofuse

Geophysical Journal International

Geophys. J. Int. (2014) **196,** 1657–1675
Advance Access publication 2013 December 20

doi: 10.1093/gji/ggt472

Acoustic response of submarine volcanoes in the Tofua Arc and northern Lau Basin to two great earthquakes

DelWayne R. Bohnenstiehl,[1] Robert P. Dziak,[2] Haru Matsumoto[2] and James A. Conder[3]

[1] *Department of Marine, Earth and Atmospheric Sciences, North Carolina State University, Raleigh, NC* 27606*, USA. E-mail: drbohnen@ncsu.edu*
[2] *Oregon State University and the National Oceanic and Atmospheric Administration, Hatfield Marine Science Center, Newport, OR* 97365*, USA*
[3] *Department of Geology, Southern Illinois University, Carbondale, IL* 62901*, USA*

Accepted 2013 November 20. Received 2013 November 19; in original form 2013 June 21

SUMMARY

Using a short-baseline hydrophone array, persistent volcanoacoustic sources are identified within the ambient noise field of the Lau Basin during the period between 2009 January and 2010 April. The submarine volcano West Mata and adjacent volcanic terrains, including the northern Matas and Volcano O, are the most active acoustic sources during the 15-month period of observation. Other areas of long-term activity include the Niua hydrothermal field, the volcanic islands of Hunga Ha'apai, Founalei, Niuatoputapu and Niuafo'ou, two seamounts located along the southern Tofua Arc and at least three unknown sites within the northern Lau Basin. Following the great Samoan earthquake on 2009 September 29, seven of the volcanoacoustic sources identified exhibit increases in the rate of acoustic detection. These changes persist over timescales of days-to-months and are observed up to 900 km from the earthquake hypocentre. At least one of the volcanoacoustic sources that did not respond to the 2009 Samoan earthquake exhibits an increase in detection rate following the great *M*w 8.8 Chile earthquake that occurred at a distance of ∼9500 km on 2010 February 27. These observations suggest that great earthquakes may have undocumented impacts on Earth's vast submarine volcanic systems, potentially increasing the short-term flux of magma and volcanic gas into the overlying ocean.

Key words: Volcano seismology; Volcanic arc processes; Backarc basin processes; Subaqueous volcanism.

1 INTRODUCTION

Repeated field surveys suggest that many submarine arc volcanoes exhibit low-level eruptive activity, magmatic degassing, hydrothermal activity and microseismicity that persist semi-continuously over multiyear timescales (e.g. Embley *et al*. 2006; Chadwick *et al*. 2008, 2012; Dziak *et al*. 2008, 2012; Resing *et al*. 2011). Yet, developing a strategy to systematically monitor these often-remote systems remains challenging. Most arc volcanoes produce few earthquakes of sufficient size to be detected by the global seismic network, and long-term *in situ* monitoring is rare in the submarine environment.

As part of an experiment to monitor seismic activity along the Eastern Lau Spreading Center (ELSC), a short-baseline four-element horizontal hydrophone array was deployed in the south-central Lau Basin, near 20.5°S, 176.75°W (Fig. 1). Beginning in 2009 January, this array tracks the directivity of the ocean noise field during a 15-month period, identifying several persistent, stationary sound sources along the volcanic Tofua Arc and within the rifted volcanic terrain of the northern Lau Basin (Fig. 1). Most of these acoustic sources align with historically active volcanic islands and seamounts that extend into the ocean sound channel, where the day-to-day low-level acoustic activity associated with a submarine volcano is most efficiently coupled into the water column.

The response of subaerial volcanoes to the static and dynamic stress changes associated with earthquakes has been well studied, and it is widely acknowledged that strong-to-great earthquakes can advance the timing of eruptions, modulate the heat flux and volumetric output during ongoing eruptions and trigger microseismicity and seismic tremor (e.g. West *et al*. 2005; Harris & Ripepe 2007; Watt *et al*. 2009). Whether or not a volcano responds depends on the magnitude of the earthquake, its distance from the epicentre, the seismic radiation pattern of the event and the eruptive history of the volcano. For a truly great earthquake, such as the *M*w 9.3 Sumatran event in 2004, the response may be global in scale (Delle Donne *et al*. 2010).

Although submarine volcanoes should respond in a similar fashion, such activity has never been documented. There are a handful of examples where regional earthquakes have been correlated with changes in the temperature or flow of hydrothermal systems in mid-ocean ridge vent fields (e.g. Johnson *et al*. 2001; Dziak & Johnson 2002; Dziak *et al*. 2003). Measurements made at an individual vent, however, may simply track local shaking-induced changes in the shallow hydrothermal network (Dziak & Johnson 2002), as opposed

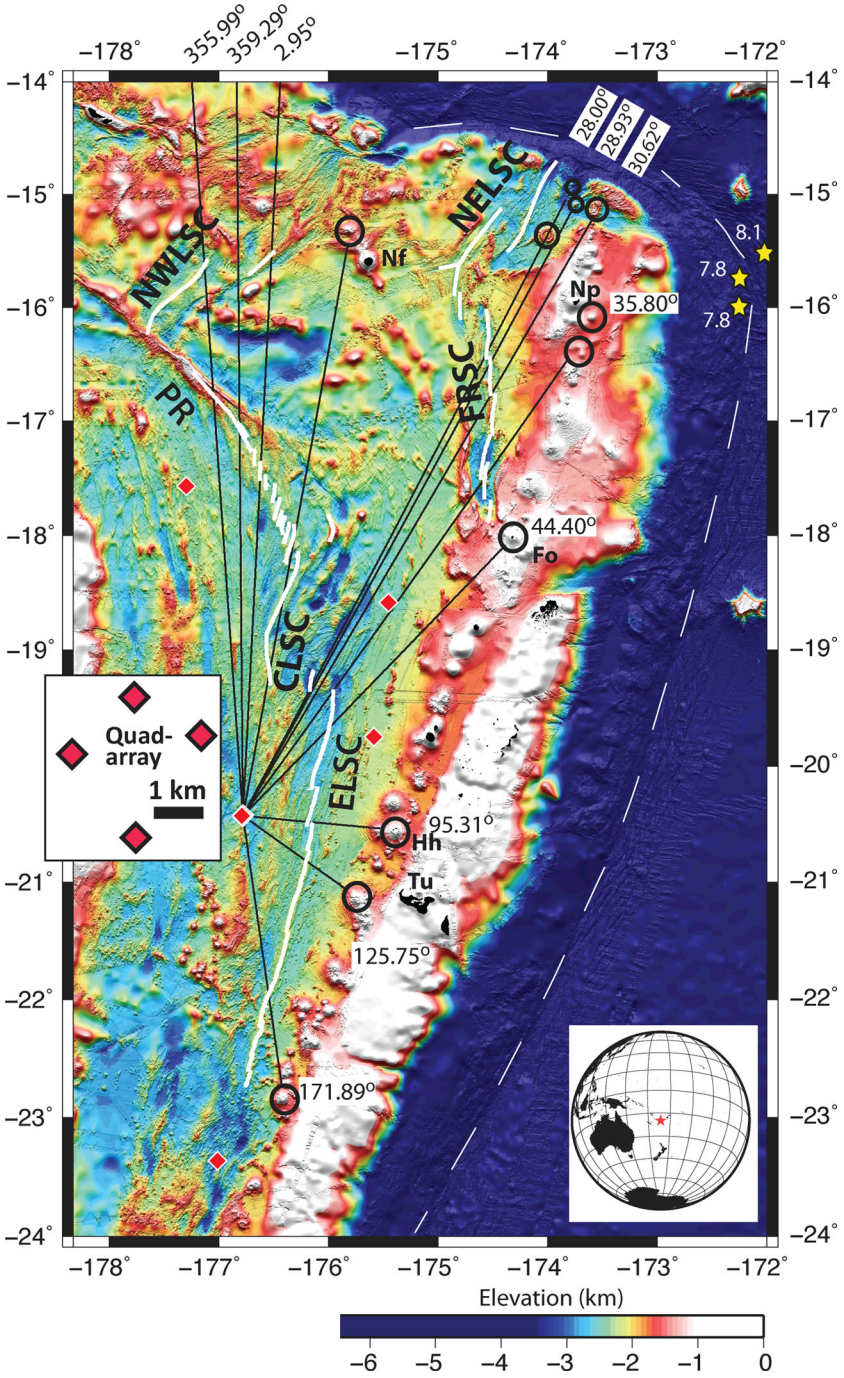

Figure 1. Regional bathymetric map and hydrophone array geometry. Red diamonds show the location of single element omnidirectional hydrophones deployed near the axis of the SOFAR channel at a depth of 1000 m below the sea surface. Central inset shows the geometry of the four-element (quad) horizontal array positioned near 20.5°S, 176.75°W. Solid lines show azimuths associated with persistent volcanic sources, and thick circles highlight the inferred source locations (Table 1). Thick white lines show the boundaries defining the Australian, Tongan and Niuafo'ou plates that comprise the Lau Basin (Zellmer & Taylor 2001). Plate boundaries are labelled as: Eastern Lau Spreading Center (ESLC), Central Lau Spreading Center (CLSC), Fonualei Rift and Spreading Center (FRSC), Peggy Ridge (PR), Northwest Lau Spreading Center (NWLSC) and Northeast Lau Spreading Center (NELSC). Thin dashed line marks the axis of the Tongan Trench. Yellow stars show the locations of the *M*w 8.1 outer rise normal faulting earthquake (2009 September 29) and two nearly coseismic *M*w 7.8 thrusts events. The islands of the Tongan chain are shaded in black and are identified as Hunga Ha'apai (Hh), Tongatapu (Tu), Fonualei (Fo), Niuatoputapu (Np) and Niuafo'ou (Nf). Bathymetry compilation courtesy F. Martinez.

to a response within the underlying magmatic system. Moreover, the statistical significance of these changes in temperature and flow has never been robustly quantified.

On 2009 September 29, an *M*w 8.1 tsunamigenic earthquake occurred on the outer rise of the Tongan subduction zone (172.25°W, 15.75°S), ∼140 km to the west of the active Tofua Arc (Fig. 1). Lay *et al*. (2010) showed that an initial normal faulting rupture was followed by two coseismic thrust events on the Tonga subduction zone, each being the equivalent of an *M*w 7.8 event. They also document widespread aftershock activity that involves underthrusting

and possible failure of the upper plate. The following year, on 2010 February 27, an *M*w 8.8 event struck off the coast of Chile—at a distance of nearly 9500 km from the Tofua Arc. This event represents the sixth largest earthquake to occur during the instrumented seismic record.

Tracking the acoustic detection rate associated with volcanoes in the Tofua Arc and northern Lau Basin provides an opportunity to systematically study the response of multiple submarine volcanoes to great earthquakes. In this paper, we evaluate the probability that the rate of acoustic detections within a given azimuthal band increases (or decreases) following the great Samoan and Chilean earthquakes. Confidence intervals quantifying the magnitude of the rate change show significant increases in acoustic detections for several of the azimuthal bands following both the Samoan and Chile events. Notably, bands responding to one do not respond to the other.

2 METHODS

2.1 Overview of instrumentation

During the period of 2009 January 20–2010 April 15, the Lau Basin hosted a short baseline (∼2 km) horizontal array of four hydrophone sensors deployed in an approximate diamond-shaped configuration (Fig. 1). Each hydrophone element was deployed autonomously, with a sensor package that consisted of a single omnidirectional ceramic hydrophone and a titanium pressure case containing a filter/pre-amplifier stage, data logging computer with an accurate clock, hard drives and an alkaline battery pack (Fox *et al*. 2001).

To take advantage of the efficient propagation of sound in the ocean, these recorders were floated near the axis of the deep sound channel (1000 ± 50 m), where they continuously sampled the ambient sound field at a rate of 250 Hz. The absolute timing for each instrument was maintained autonomously using a QT2001N® temperature-correcting Microprocessor Controlled Crystal Oscillator clock (MCXO) manufactured by Q-tech Corporation (Culver City, CA, USA) that was calibrated by GPS time before and after deployment. Measured absolute drift rates ranged between 90 and 420 ms yr^{-1}. At all four hydrophones, in addition to the acoustic channel, the clocks' one pulse-per-second (1-PPS) signal was logged continuously and post-processed for more precise timekeeping. Timing errors resulting from long-term clock stability were minimized using a linear time drift assumption.

The quad-array instrumentation was part of a larger (five-station) network of autonomous hydrophones deployed to monitor shallow earthquakes along the ELSC (Fig. 1). Traditionally, acoustic *T*-wave arrival times recorded at distant stations such as these would be used to solve for source location and origin time. Location accuracy, however, degrades quickly outside of the network for solutions derived using this single seismoacoustic phase (Fox *et al*. 2001). Moreover, in this setting, the shallow bathymetry along the Tofua Arc may restrict certain source–receiver paths, limiting the number of observed arrivals. As an alternative to this event-based processing, we adopt a correlation-based detector that uses only data from the small-aperture quad array positioned near the longitudinal centre of basin (Fig. 1). This approach catalogues coherent, small-amplitude acoustic arrivals that may be difficult to detect and associate across the larger network (e.g. Schaff 2008). It also easily incorporates signals with variable time-frequency characteristics into the detection record; whereas, some volcanoacoustic noise (e.g. tremor) might be poorly accounted for through traditional event-based cataloguing.

2.2 Quad-array processing and assessment

The quad array is used to estimate the backazimuth of incoming acoustic energy using a plane wave fitting routine (e.g. Del Pezzo & Giudicepietro 2002; Chapp *et al*. 2005). The traveltime differences between hydrophone pairs (t_{ij}) are estimated from the cross correlation of their low-frequency (2–20 Hz) bandpassed waveforms. The horizontal slowness is found by solving the system of equations $\Delta p = t$, where Δ represents a two-column matrix containing the offsets in the *x*- and *y*-directions between sensor pairs, t is a column vector of the corresponding time delays and the vector p represents the two-component (p_x, p_y) horizontal slowness. The velocity (v) and azimuth (az) are given as $v = 1/|p|$ and $az = \tan^{-1}(p_x/p_y)$. Reported backazimuths are assessed for quality based on the correlation coefficient (cc) between stations pairs, the closure value estimated by summing the lags ($cl = t_{12} + t_{23} + t_{34} + t_{41}$), which should be near zero and the velocity (v) returned by the inversion, which is expected to be ∼1.485 km s^{-1} for acoustic waves travelling within the low-latitude sound channel.

The results presented here use a correlation window length of 8 s where the analysis window is advanced in 1-s time steps. An acoustic detection is declared for windows reporting $cc > 0.55$, $|cl| <$ 48 ms and v = 1.485 ± 0.075 km s^{-1}. Cross correlations are derived using the low-frequency 2–20 Hz bandpassed waveforms. The high-pass cut-off excludes low-frequency ocean noise and possible cable strumming. The low-pass cut-off is applied to filter possible marine animal vocalizations (Brodie & Dunn 2011) and noise sources associated with shipping traffic (Fig. 2d) and other anthropogenic activity.

The absolute accuracy of the azimuth calculation was verified by using a series of seismic airgun shots produced using the 'R/V Langseth' between 2009 January 27 and February 24 (Dunn & Martinez 2010; Bohnenstiehl *et al*. 2012; Dunn *et al*. 2013). The survey deployed thousands of acoustic sources along the ELSC at ranges between 30 and 100 km from the quad array and at backazimuths between 80° and 135°. Due to the bottom-limited sound velocity structure of the Lau Basin (Bohnenstiehl *et al*. 2012), these near-surface shots propagate largely via seafloor scattering and bottom reflection—unlike volcanic sources, which may couple directly into and propagate as refracted energy within the sound channel. This strong bottom interaction is expected to degrade the azimuthal resolution; nonetheless, for those shots that have return arrivals meeting the detection threshold outline above (i.e. $cc > 0.55$, $|cl| < 48$ ms, $v = 1.485 \pm$ 0.075 km s^{-1}), the deviation of the estimated azimuth from the true azimuth shows a normal distribution with a mean offset of 0.25° counter-clockwise and 0.37° standard deviation. Bohnenstiehl *et al*. (2013) demonstrates the use of azimuthal detection data in localizing the volcanoacoustic signals associated with the 2009 March eruption of Hunga Ha'apai Hunga-Tonga volcano, which lies just outside of the ELSC hydrophone network (20.57°S 175.35°W; Fig. 1).

By setting these thresholds for declaring an acoustic detection reasonably high, *T*-wave energy associated with earthquakes along the subduction interface and within the downgoing slab are effectively excluded from the detection process. To reach the quad array in the backarc, seismic energy from earthquakes along the subduction interface must propagate through a significant section of the arc crust, before coupling into the sound channel along a broad section of the west-facing slope of the Tonga Ridge. Consequently, these arrivals are not well represented as a plane wave and few-to-no detections are declared (Fig. 2a). *T* waves generated by

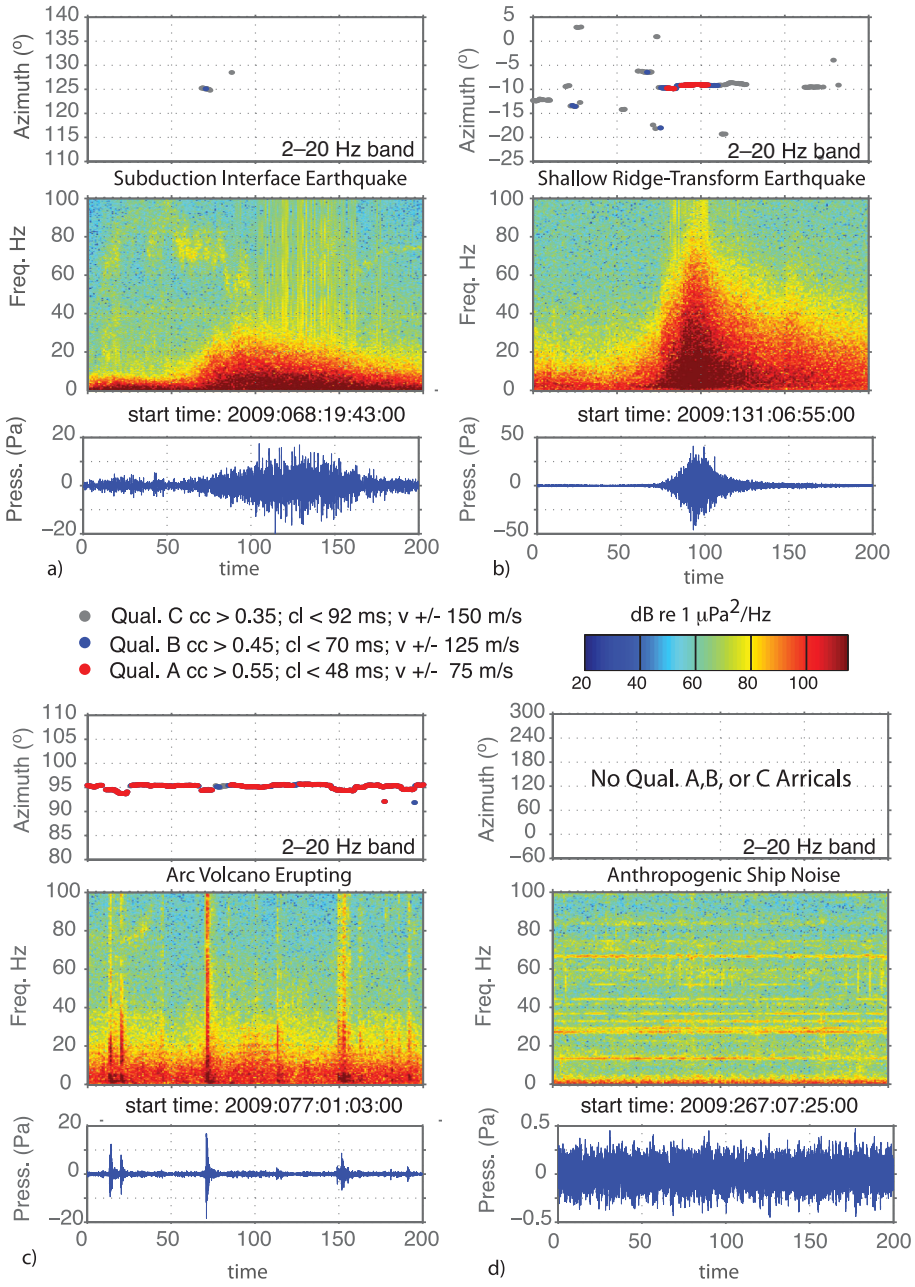

Figure 2. Response of the quad-array correlation detector to common geoacoustic signals observed within the Lau Basin. For each example, the bottom and middle panels show the acoustic pressure time-series and corresponding spectrogram, respectively. The top panel shows the colour-coded correlation as a function of time and backazimuth. Time windows with correlations exceeding the detection threshold ($cc > 0.55$, $|cl| < 48$ ms, $v = 1485 \pm 75$ m s^{-1}) are coloured in red and labelled as Quality A. (a) *T*-wave arrival associate with a 5.0 M_b thrust-faulting earthquake along the shallow Tongan subduction interface, near 21.86°S, 175.10°W on 2009 March 29 (ISC 2011). Such signals are characterized by dominantly low-frequency energy, reflecting the long land path prior to *T*-wave conversion. As seen in this example, they commonly produced few, if any, detections (red dots) due to the fact that the arrivals typically represent a summation of energy sourced from along a broad section of the arc. (b) A *T*-wave arrival associated with a shallow hypocentre 4.4 M_b earthquake along the Peggy Ridge at 16.19°S, 177.66°W on 2009 May 11 (ISC 2011). *T* waves generated by shallow hypocentre earthquakes within the basin or Tofua Arc commonly produce detections associated with the time of peak *T*-wave amplitude. (c) Continuous low-frequency tremor and broad-band volcanic explosions associated with the eruption of HungaTonga-Hunga Ha'apai volcano (20.57°S, 175.38°W) in 2009 March (Vaughan & Webley 2010; Bohnenstiehl *et al*. 2013). Note the sustained detections (red dots) as the signals emanating from this shallow volcanic structure coupled effectively into the sound channel. (d) Example of anthropogenic shipping noise, which is characterized by sustained constant frequency tones. These signals are comparatively low amplitude (note changing pressure scale between panels), and typically produce few-to-no detections. Moreover, since ships are moving targets, they do not produce persistent stationary detection bands like those associated with volcanic centres.

subduction zone earthquakes are typically spindle shaped and deficient in high-frequency energy (Fig. 2a).

By comparison, shallow-hypocentre earthquakes, which are associated with spreading centres in the backarc and active volcanoes along the arc, produced *T* waves with more symmetric arrival patterns and broad-band spectrum (Fig. 2b). For these 'abyssal' *T* waves (*cf.* Johnson *et al*. 1968), the area of acoustic conversion at the seafloor scales with the depth of the earthquake, but the region of

peak *T*-wave excitation is found to lie proximal to the epicentre (*cf.* Schreiner *et al*. 1995; Slack *et al*. 1999; Yang & Forsyth 2003). Relative to subduction-zone generated *T* waves, these abyssal *T* waves better approximate a point source within the basin. The quad array therefore records a set of acoustic detections typically associated with the amplitude peak within the *T*-wave arrival (Fig. 2b).

Volcanic signals (e.g. explosions, tremor and *T* waves) originating from shallow arc volcanoes can couple directly into the sound channel and therefore propagate efficiently across the basin. During periods of significant volcanic unrest or during a seafloor eruption, the detector may be triggered in a semi-continuous manner (Fig. 2c).

3 IDENTIFICATION OF PERSISTENT VOLCANOACOUSTIC SOURCES

Fig. 3 shows a plot of acoustic detections (as defined in Section 2.2) verses azimuth. As expected, there are few detections arriving from the west of the quad array, reflecting the fact that the western margin of the Lau Basin is tectonically passive. Most of the detections arrive from the northern Lau Basin, which hosts a network of spreading centres that accommodate rapid backarc extension (e.g. Zellmer & Taylor 2001), and the Basin's active eastern margin, which boasts the fastest plate convergence rates on Earth (Bevis *et al*. 1995) and includes a number volcanic centres with documented activity over Holocene to historic timescales (Siebert *et al*. 2010).

Within this time versus azimuth representation of the detection data, a number of persistent bands emerges—generating a series of horizontal stripes in Fig. 3. Table 1 identifies the 12 most prominent bands. In a histogram representation of the detection azimuths (Fig. 4), these detections cluster into roughly normally distributed peaks with standard deviations of only a few tenths of a degree (Table 1). This suggests that they are associated with a single stationary source, or a tightly clustered set of sources. Projecting these azimuthal bands backwards from the quad array, nine of the bands align with known or inferred volcanic centres (Fig. 4) and the remaining three appear to be associated with sources within the largely unexplored volcanic terrain of the north-central Lau Basin (Fig. 1).

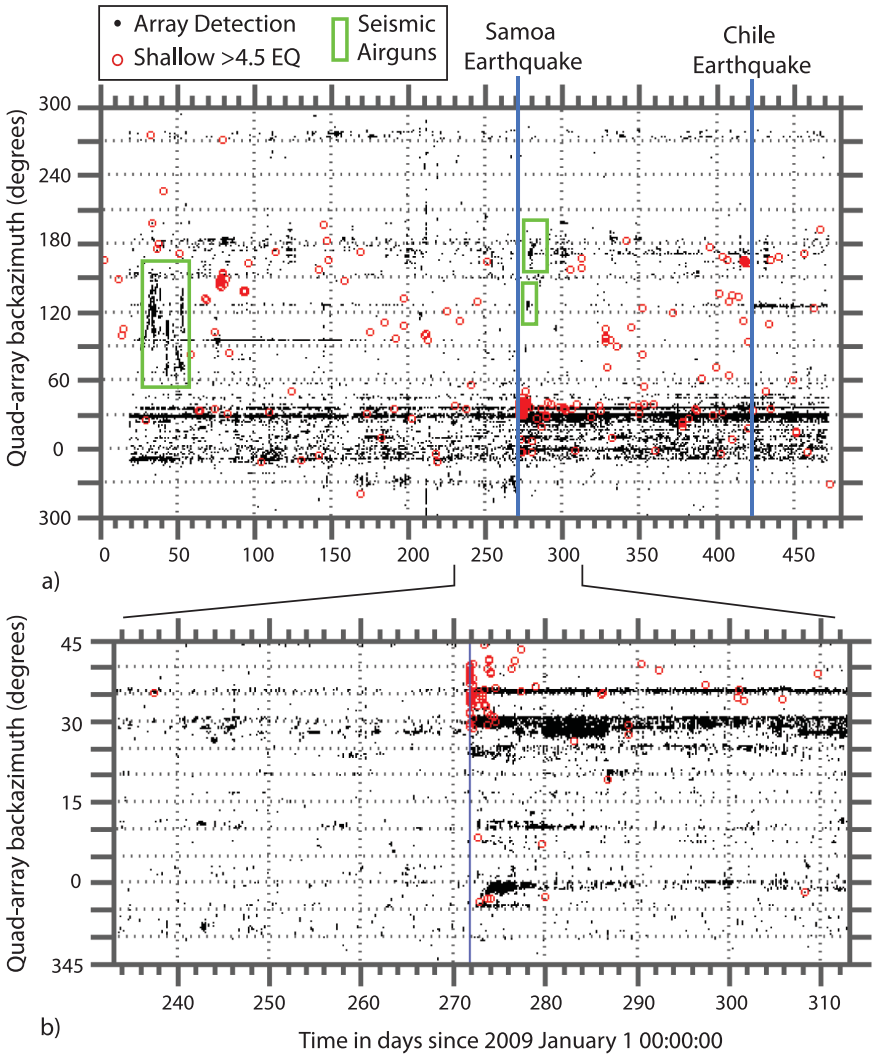

Figure 3. Time versus azimuth plot with black dots indicating plane wave detections on the quad array, where detections are defined to be Quality A correlations with $cc > 0.55$, $|cl| < 48$ ms, $v = 1485 \pm 75$ m s^{-1}. Horizontal stripes represent persistent sources of underwater acoustic noise. Red circles mark the time and azimuth of shallow >4.5 *M* earthquakes that occurred during the deployment (ISC 2011). (a) Basin scale view of the entire monitoring period, with times of the 2009 Samoan and 2010 Chile earthquakes marked by vertical blue lines. Green boxes highlight air-gunning activity in the basin. (b) View of detections originating from the N–NE direction in the weeks before and after the 2009 Samoan earthquake. Note that although the aftershock field is distributed broadly between 27° and 47° azimuths, detections are more narrowly focused primarily in the same bands observed to persist prior to the Samoan earthquake.

Table 1. Summary of persistent acoustic sources in Lau Basin.

Mean azimuth	Standard dev.	No. detect.	Per cent detect.	Acoustic source
2.95	0.23	3479	0.23	Unknown
10.53	0.38	8143	0.53	Niuafo'ou Is. Platform
28.00	0.16	337 881	22.29	Volcano O/North Matas
28.93	0.17	883 489	58.29	West Mata Smt.
30.62	0.16	14 480	0.96	Niua
35.80	0.12	42 168	2.78	Niuatoputapu Is. Platform
44.40	0.24	11 795	0.78	Founalei Is.
95.31	0.48[a]	192 840	12.72	Hunga Ha'apai Is.
125.75	0.57[b]	4821	0.32	Volcano 1 Smt. 21°10′S, 175°45′W
171.89	0.24	596	0.04	Pelorus Reef Smt. 22°50′S, 176°25′W
355.99	0.19	2963	0.20	Unknown
359.29	0.56	12 977	0.86	Unknown

[a]Data can be fit with bimodal distribution of azimuths with peaks at 94.7° and 95.7° representing presence of two eruptive vents posited along the north and south coasts of the island (Vaughan & Webley 2010; Bohnenstiehl *et al*. 2013).
[b]Data can be fit with bimodal distribution with peaks at 125.25° (*T* waves) and 126.25° (long-duration, low-frequency signals).

The detection bands represent signals with variable time-frequency characteristics, as discussed later. Notably, the observed bands are not associated with the more populated islands, where ship traffic and coastal construction activities are most intense (e.g. Tongatapu Island). Therefore, anthropogenic noise is an unlikely explanation for these persistent acoustic sources. Moreover, since there are many more small islands and shallow atolls, located at varying backazimuths, than detections bands, these persistent acoustic sources are not likely to originate from wave-breaking, sound producing marine animals or other oceanographic phenomena associated with shallow bathymetry.

3.1 West Mata, the Matas and Niua volcanoes

The band with by far the largest number of detections is centred at 28.93°N (Fig. 4a). This azimuth passes direct over the western shoulder of West Mata Volcano—an elongated, east–northeast trending, cone-shaped edifice that resides ∼20 km to the west of the main volcanic arc. It is constructed principally of Boninite lavas that require unusually hot, hydrous shallow mantle conditions. Repeated observations of West Mata have shown that it erupts semi-continuously at a low (VEI 0) level (Resing *et al*. 2011). Its summit elevation lies at ∼1200 mbsl, near the axis of the SOFAR channel where the coupling of low-level acoustic noise into the ocean waveguide is the most efficient (Matsumoto *et al*. 2011).

Slightly counter-clockwise from West Mata, at an azimuth of 28.00°, lies the northern Matas volcanic complex (Fig. 4a). The core of the Matas volcanic complex is constructed from seven en echelon cones that have elongated shapes and Boninite lava compositions similar to West Mata (Resing *et al*. 2011). The summit peaks lie at slightly deeper depths, ∼1850 mbsl, but are still well within the deep sound channel. The Matas have been identified as an area of intense hydrothermal activity, with at least five high-temperature vent sites (Resing *et al*. 2011).

This same 28.00° azimuth, however, also passes over Volcano O caldera (also known as NE Lau Caldera, MTJ-1 Volcano; Fig. 4a). This area is known to host a major hydrothermal system, with elevated Fe/Mn ratios in the hydrothermal plume that are related to magmatic fluids. Moreover, native sulphur and alunite in seafloor samples suggest the outgassing of magmatic SO_2 (Kim *et al*. 2009). Using the azimuthal detection data alone we are not able to distinguish between acoustic sources associated with the Matas and Volcano O. Given evidence of robust magmatic–hydrothermal systems associated with both volcanic edifices, this detection band may well represent a composite of both source regions. The number of detections within this band makes it the second most active throughout the monitoring period (Table 1).

To the west of West Mata, at an azimuth of 30.62° from the quad array, lies the Niua Volcano and hydrothermal field. Although much less active than the Matas (Fig. 4a), the azimuthal pattern of detections shows a distinct peak associated with this broad shallow topographic feature. Unlike West Mata, Niua is positioned along the trend of the main Tofua volcanic arc. Niua has an irregular north–northeast trending base with local peaks in both the north and south. Hydrothermal venting at southern Niua was discovered by a commercial survey in 2008. It consists of two subareas at depths of ∼900 and ∼1180 mbsl that are separated by ∼1.3 km along the rim of a crater-like depressions (Nautilus Minerals Inc. 2008). In the north, a seafloor dredge has recovered recently molten sulphur from a depth of ∼750 mbsl—indicating a shallow gas-charged magma chamber (National Oceanic and Atmospheric Administration 2012).

Signals emanating from the 28.00° (the Matas/Volcano O) and 28.93° (West Mata) bands show a great diversity of signal types, many having characteristics typically associated with submarine volcanism (Fig. 5). West Mata produces a range of broad-band acoustic pulses with sharp onset and end times (Fig. 5a) and a suite of poly- and monochromatic gliding tremor signals that exhibit variable fundamental frequencies (Figs 5a–c). Both 28.93° and 28.00° bands also produce short-duration broad-band acoustic spikes (Fig. 5d) with time-frequency characteristics that resemble the shallow phreatomagmatic explosions observed during the eruption of Hunga Ha'apai (*cf*. Fig. 2c).

3.2 Hunga Ha'apai

The band with the third largest number of detection is directed towards Hunga Ha'apai Island Volcano (Tables 1 and 2), which underwent a surtseyan (VEI 2) eruption during the period 2009 March 16–19 (Vaughan & Webley 2010; Bohnenstiehl *et al*. 2013). During the eruption, the volcano produced a large number of detections associated with low-frequency tremor activity and a series of explosions (Fig. 2c). Bohnenstiehl *et al*. (2013) identified the volcano as an active acoustic source from the time monitoring began in 2009 January (Fig. 3a). After the eruption, acoustic activity is sustained

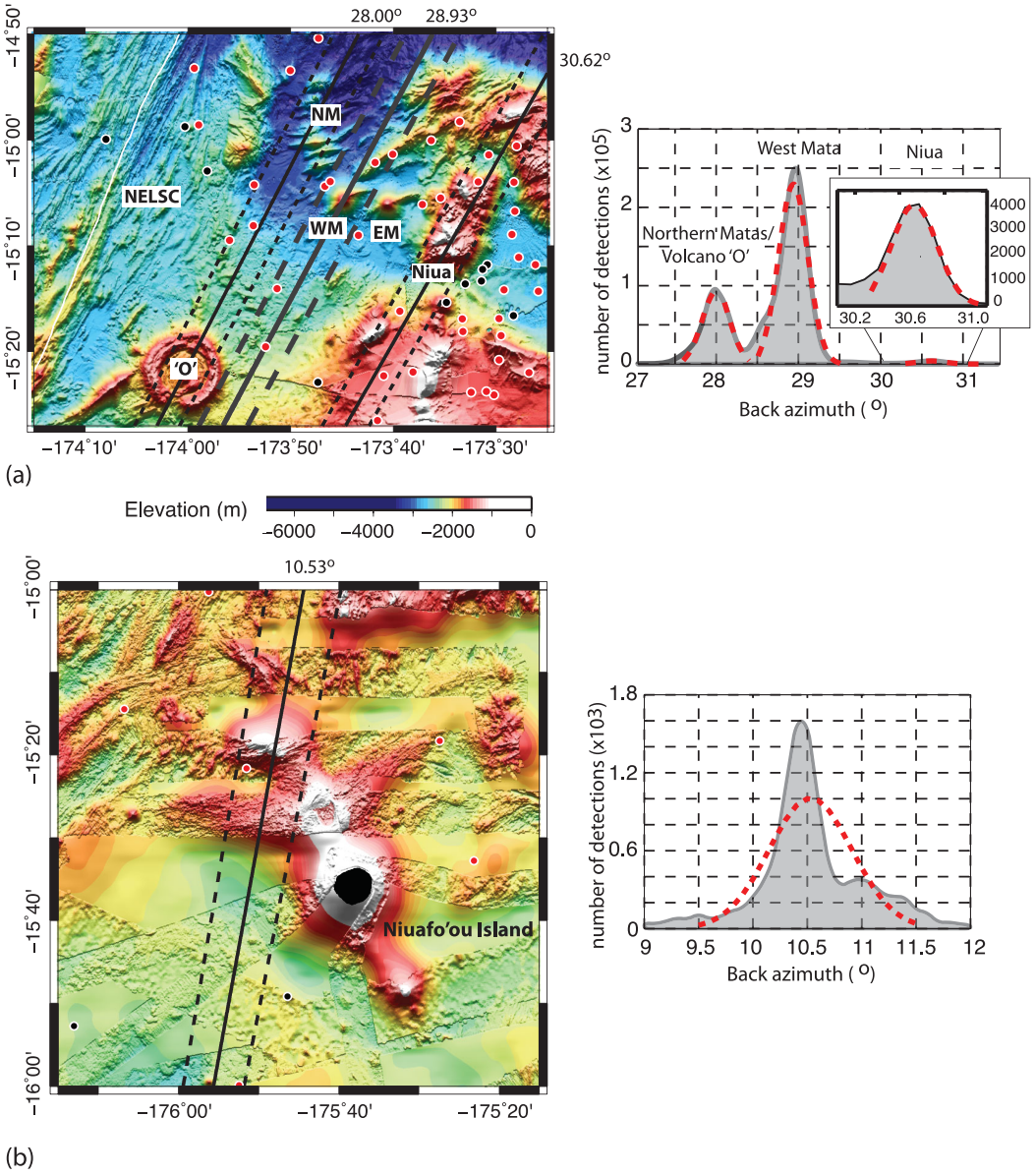

Figure 4. Left-hand panels: Projected source locations for the primary detection bands for which the source region can be inferred. Solid grey lines shown mean azimuth within the detection band; dashed lines show two standard deviation limits. Dots show shallow $M \geq 4.5$ earthquakes that occurred during the monitoring period (ISC 2011). Black dots represent earthquakes that occurred before the 2009 September Samoan earthquake; red dots indicate those that occurred after this event, including its aftershocks. Right-hand panels: Azimuth histograms are fit with a unimodal normal distribution (red). Geographic regions shown are for azimuths associated with (a) West Mata (WM) at 28.93°, the northern Matas (NM)/Volcano O at 28.0° and Niua hydrothermal field at 30.62°. Also labelled are the inactive East Mata seamount (EM) and the Northeast Lau Spreading Center (NELSC); (b) Niuafo'ou Island Platform at 10.53° azimuth; (c) The region south of Niuatoputapu Island at 35.80° azimuth, (d) Fonualei Island at 44.40° azimuth; (e) Volcano 1 seamount near 21°10′S, 175°45′W at 125.75° azimuth; (f) Pelorus seamount near 22°50′S, 176°25′W at 171.89° azimuth.

at above background levels as steam eruptions and degassing continues, but the rate of detection decreases steadily over a period of several months, with the volcano becoming acoustically dormant by mid-summer of 2009. Bohnenstiehl *et al*. (2013) describe the temporal evolution of the acoustic signals associated with this eruption in detail.

3.3 Niuafo'ou Island Platform

The island of Niuafo'ou is built upon a broader volcanic platform that extends to the northwest from the island (Fig. 4b). The doughnut-shaped island contains a steep-sided lake filled caldera with a rim that rises up to an elevation of 250 m. It has erupted at least 12 times since 1814. The largest eruption (VEI 4) occurred along the NE side of the caldera in 1886, and it erupted most recently within the NE portion of the caldera lake in 1985 (VEI 0) (Siebert *et al*. 2010).

The detection histogram shows a local maximum centred at 10.53°, which corresponds to an unnamed submarine peak located at the NW limit of the volcanic platform upon which the island is built. The azimuthal distribution of detections is skewed clockwise from this peak towards the island itself (Fig. 4b). The signals associated with the Niuafo'ou Island Platform are dominantly shallow-hypocentre abyssal *T* waves.

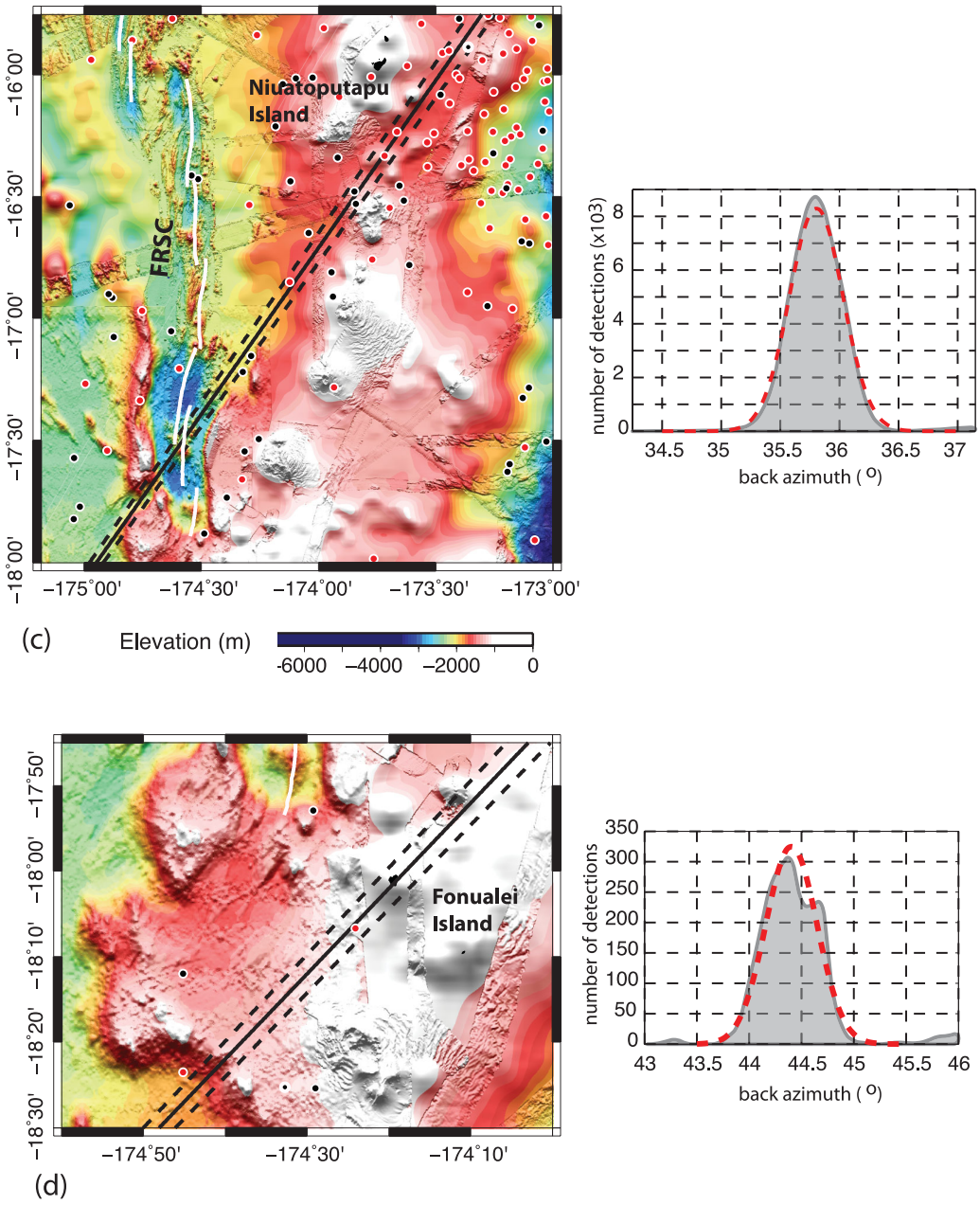

Figure 4. (*Continued.*)

3.4 Submarine centre(s) near Niuatoputapu Island

The azimuth band centred at 35.80° passes to the south of Niuatoputapu Island. Niuatoputapu is a flat-lying reef-rimmed island built upon an eroded volcanic edifice. Although Niuatoputapu is extinct, last erupting at ∼3 Ma, it is neighboured to the north by Tafahi Island, a steep-sided likely Holocene age volcanic cone, and to the north and south by a number submarine edifices that likely represent active volcanic centres (Siebert *et al*. 2010). Taylor (2003) speculates that rafted pumice observed in 2002 October may have been sourced from one of these active centres south of Niuatoputapu.

Acoustic signals emanating from the seafloor adjacent to Niuatoputapu Island must cross the steep flank topography of the Fonualei Rift Spreading Center (FSCR; Fig. 4c). The 35.80° azimuth band is unique in that the acoustic path exploits a narrow wind-gap-like slit across the rifts' flanks. This may explain the shape of the detection histogram, which is extremely narrow (0.12°) and highly symmetric (Fig. 4c). The acoustic signal detections within this band are dominantly low frequency (<40 Hz), long duration arrivals, which would be consistent with stronger seafloor interaction across the shallow Tofua Arc and Fonualei Rift.

3.5 Founalei Island

Fonualei is a small (<2 km diameter) island that contains an active fumarolic crater. Seven eruptions have been recorded since 1791. The largest (VEI 4) eruption occurred in 1846 June, when explosive volcanism produced large pumice rafts and an ash fall that damaged crops 56 km away on the island of Vavau and fell on vessels at a range of 950 km. The most recent activity occurred in 1974 February, when small quantities of steam, foam and rocks were emitted all

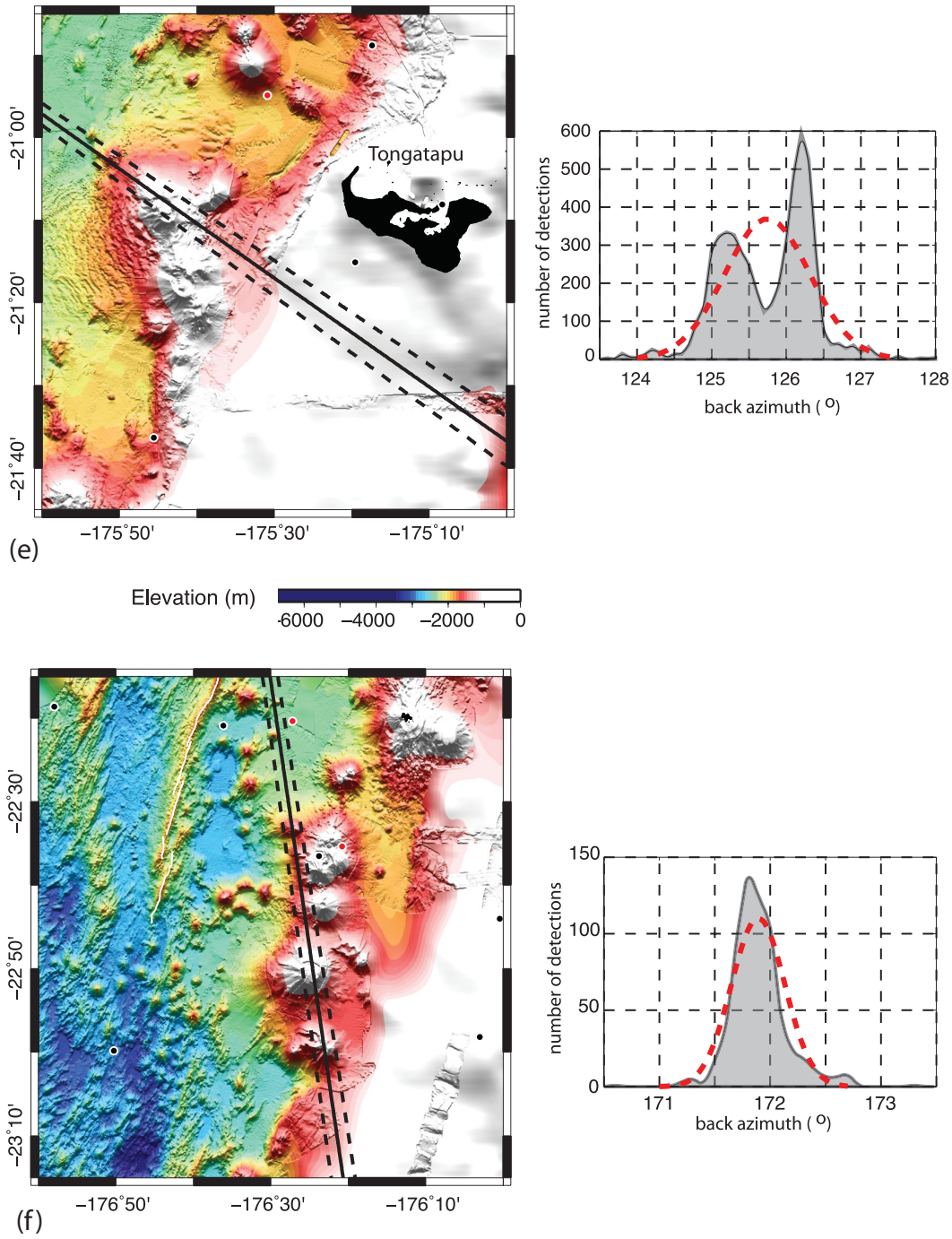

Figure 4. (*Continued.*)

around the crater (Siebert *et al*. 2010). Although the 44.40° azimuth band shows limited activity relative to the sources discussed earlier (Table 1), detections form a clear peak centred on the small island (Fig. 4d). The detections are dominated by shallow abyssal-type *T* waves.

3.6 Seamount near 21°10′S, 175°45′W (Volcano 1)

A band of activity is aligned with the northern most cone in a cluster of seamounts located ∼50 km to the west–southwest of Tongatapu Island (Fig. 4e). This cone, previously designated as Volcano 1, rises to ∼65 mbsl at its shallowest depth (Stoffers *et al*. 2003, 2006; Hekinian *et al*. 2008; Kim *et al*. 2013). Volcano 1 is believed to be associated with a documented submarine eruption in 1906, which produced pumice rafts and ejected pyroclastic material 100 m into the air. A second eruption in this area was reported in late 1932 (Richards 1962; Siebert *et al*. 2010).

Analysed lavas from Volcano 1 are mostly of andesitic composition, with a stratigraphy developed from repeated small eruptions of pyroclastic material, occasional outpourings of lava and the deposition of material during small-scale collapses (Hekinian *et al*. 2008; Kim *et al*. 2013). Detailed bathymetric mapping shows a large (4.5 × 7 km) oval-shaped caldera with a floor at a depth of

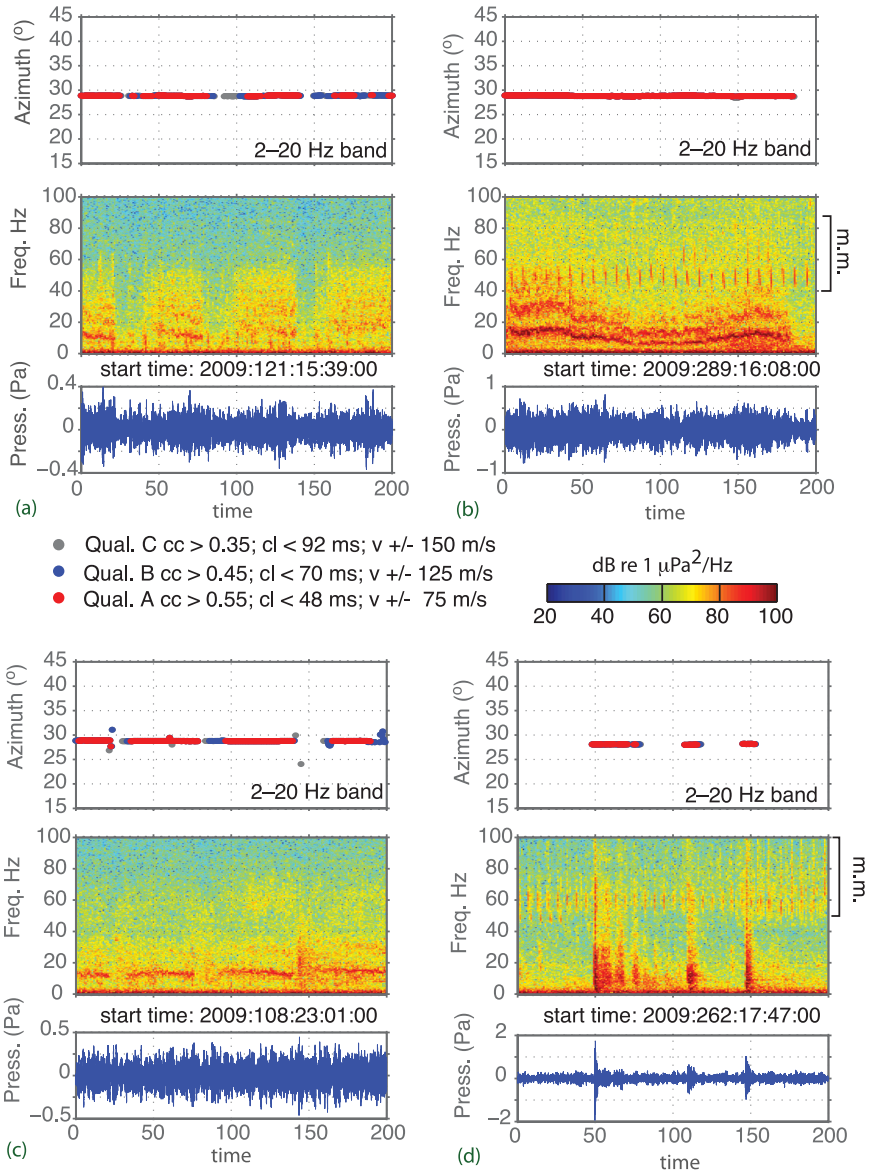

Figure 5. Example signals associated with detections originating from the Matas/Vol. O and West Mata. (a) Broad-band bursts lasting tens of seconds with weak harmonics, (b) Gliding polychromatic tremor, (c) Monochromatic tremor and (d) Impulsive explosions and shallow *T* waves. Portions of the spectrograms (b) and (d) exhibiting marine mammal vocalizations are identified (m.m.) on the right vertical axis.

~450 mbsl and a rim height of 200–300 m. Near the western margin of the caldera there are two well-preserved scoria cones, one of which is marked by explosion craters that are up to 100 m deep (Stoffers *et al*. 2006; Hekinian *et al*. 2008). Submersible data indicate widespread diffuse hydrothermal venting and vigorous gas discharge (Stoffers *et al*. 2006; Hekinian *et al*. 2008).

Unlike most other detections bands, the azimuths are strongly bimodal, with one peak near 125.25° and the other near 126.25°. This 1° angular separation translates to a separation of only 1.8 km at the range of the volcanic arc. The base of the volcanic cone, however, is much wider, on the order of 15 km across (Fig. 4f) and therefore the peaks are associated with different source areas on the same edifice. The band centred at 126.25° is made up of short-duration *T* waves associated primarily with a swarm that occurred on 2009 May 26 (Fig. 6a). The 125.25° detection band is made up of long-duration, low-frequency signals (<15 Hz) that begin on 2010 February 27 following the passage of seismic waves associated with the great Chilean earthquake (Fig. 6b). This is the only instance where a distinct change in signal character is seen before and after one of the great earthquakes. As this seamount lies proximal to the array along its eastern edge, the larger hydrophone network adds additional constraints on the source location. *T*-wave arrivals associated with the 2009 May swarm shown in Fig. 6(c) also verify the association with the seamount.

3.7 Seamount near 22°50′S, 176°25′W (Pelorus Reef)

The detection band with the smallest number of events falls at an azimuth of 171.89°. This acoustic path crosses a volcanic cone within the Tofua Arc near 22°50′S, 176°25′W, in an area identified as Pelorus Reef on some nautical charts. The cone is symmetrical and capped by a ~5-km diameter caldera with a floor at a depth of ~600 mbsl and ~100 m tall rims. Post-caldera volcanism has built

Table 2. Rate changes before and after the 2009 Samoan earthquake.

Az. band	$T_b = 252.7$ d $T_a = 200.3$ d		$T_b = T_a = 10$ d		$T_b = T_a = 20$ d		$T_b = T_a = 40$ d	
Table key →	N_b N_a	$r_{90\text{ per cent}}$	N_b N_a	$r_{90\text{ per cent}}$	N_b N_a	$r_{90\text{ per cent}}$	N_b N_a	$r_{90\text{ per cent}}$
2.95	1219 2260	**2.26–2.51**	52 101	1.51–2.76	70 118	1.51–2.26	100 146	1.26–2.01
10.53	1978 6165	**4.01–4.26**	28 3285	**85.5–158.8**	124 3800	**26.51–035.76**	341 3890	**10.51–12.76**
28.00	6350 331 531	**64.76–67.51**	2121 40 559	**18.51–20.01**	4609 120 614	**25.76–27.01**	4681 120 691	**25.26–26.51**
28.93	117 219 766 270	**8.26–8.51**	109 2300	**18.01–24.76**	233 45 284	**174.5–216.5**	2755 71 543	**25.26–27.01**
30.62	911 13 569	**18.01–20.01**	22 3454	**110.0–220.0**	110 4717	**36.76–52.26**	554 5739	**9.76–11.26**
35.80	5174 36 994	**9.01–9.26**	231 12 409	**48.26–60.01**	383 15 058	**36.26–43.01**	713 19 764	**26.26–29.51**
44.40	760 1035	1.76–2.01	83 42	0.51–0.76	106 54	0.54–0.76	169 60	0.45–0.57
95.31	192 827 13	$\sim 10^{-4}$	0 0	N/A	0 0	N/A	7 0	N/A
125.75	2552 2269	1.16–1.37	Air-gunning		14 6	0.26–1.01	20 6	0.26–0.76
171.89	79 517	**6.06–10.26**	Air-gunning		25 39	1.26–2.51	37 69	1.51–2.76
355.99	732 2231	**3.76–4.26**	34 1325	**29.26–51.51**	54 1341	**19.76–31.26**	113 1360	**10.26–14.26**
359.29	1545 11 432	**9.01–10.01**	78 5641	**60.01–87.04**	189 6257	**29.51–37.51**	261 7608	**26.5–32.51**

Note: Bold values indicate positive rate changes with $r_{90\text{ per cent}} > 2$.

two cones along the western margin of the caldera, with peaks that rises to depths of 50 and 35 mbsl (Stoffers *et al*. 2003). There are no historical eruptions reported in this area; however, the volcano is distal to the Tongan Island chain and therefore ship and air traffic (necessary to spot small eruptions) are likely sparse. The 171.89° detection band is silent until 2009 July 24 (JD 205), and then remains active throughout the monitoring period. The signals are abyssal-style *T* waves with sharp onsets and very small amplitudes.

3.8 Unknown sources within the northern Lau Basin

Although it is less well explored and more poorly mapped, the northern Lau Basin is known to host a number of seamounts and spreading ridge segments (e.g. Taylor *et al*. 1996), including the seismically active Peggy Ridge (Eguchi *et al*. 1989; Conder & Wiens 2011). Therefore, many coherent *T*-wave arrivals originate from the northern basin; however, only three bands of activity appear as distinct sound sources forming narrow histogram peaks (Table 1) that persist throughout the monitoring period. These occur at azimuths of 2.95°, 355.99° and 359.29°. Detections within these bands are dominated by shallow-hypocentre *T* waves. All three azimuths cross the Peggy Ridge, portions of the Northwest Lau Spreading Center and several large seamounts evident in the satellite derived bathymetry (Fig. 1). Consequently, the azimuthal constraints do not allow us to associate these sources with a specific volcano. The persistent character and localized nature of these bands, however, are similar to those associated with isolated volcanoes along the arc. This distinguishes these signals from the background *T*-wave sources associated with tectonic earthquakes along plate boundaries to the north of the array.

3.9 Excluded sources

Monowai Volcano is located along the Kermadec Arc near 25°53′S, 177°10′W at an azimuth of ∼183° from the quad array. Monowai has sourced numerous historical eruptions and has a well-documented history of cone building and debris flows (Wright *et al*. 2008; Watts *et al*. 2012). Throughout the 15-month monitoring period, Monowai produces periodic episodes of activity that last days-to-weeks, making it a persistent acoustic source. However, because the acoustic propagation path from Monowai to the quad array parallels the shallow bathymetry of the volcanic arc, the arrivals are weakly coherent ($cc < 0.55$) with signal azimuths that indicate significant scattering and reflection from the arc. Our correlation-based detector approach therefore does not provide a complete accounting of Monowai's activities, and it alone cannot definitively separate Monowai from nearby sources to its north. We therefore do not consider the rate of acoustic activity associated with Monowai in this assessment.

4 VOLCANOACOUSTIC RESPONSE TO GREAT EARTHQUAKES

4.1 Overview

The most active sources of acoustic noise identified in Section 3 are associated with recently active submarine volcanoes. In the

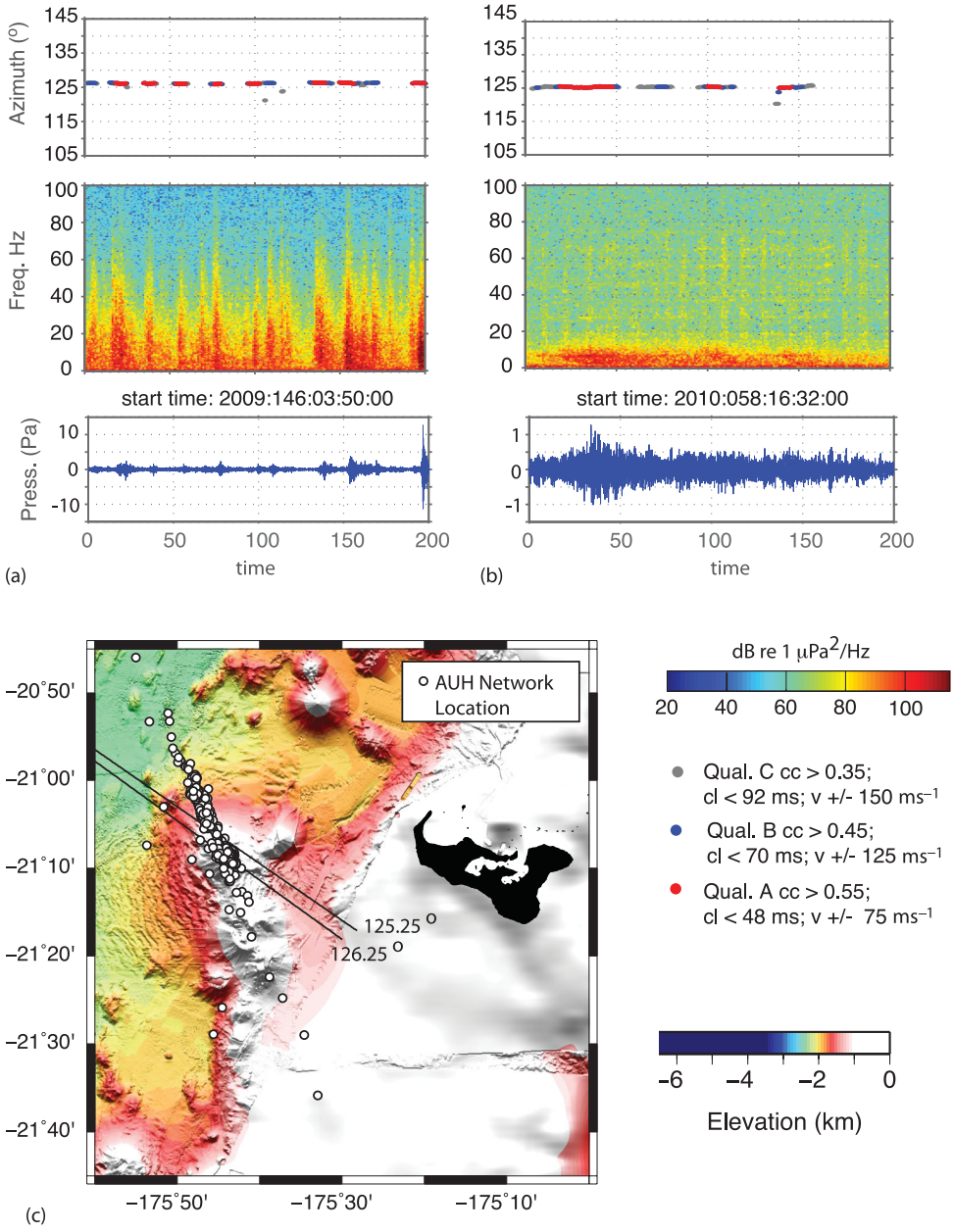

Figure 6. Two types of acoustic signal detections associated with the Volcano 1 seamount (21°10′S, 175°45′W). (a) Signals before the Chilean earthquake, including a large swarm of earthquakes on JD 146 2009, are shallow *T* waves that arrive at an azimuth of 126.25°. (b) Within 1.8 hr of the Chilean earthquake, a pronounced long-duration low-frequency signal is observed and continues intermittently throughout the rest of the deployment. These signals arrive at an azimuth of ∼125.25°. (c) Map of Volcano 1 seamount showing that azimuths associated with both signal types projected back to the western most cone in the seamount complex. Circles show *T*-wave locations derived from the five-station network of autonomous sensors, most of which occurred on JD 146. The seamount lies just outside the array and the epicentres are distributed along an azimuth that points back to its geometric centre.

case of West Mata, there is clear evidence for sustained low-level (VEI 0) activity (Resing *et al*. 2011) and Hunga Ha'apai erupted spectacularly over a period of several days in 2009 March (Vaughan & Webley 2010; Bohnenstiehl *et al*. 2013). Most of the remaining bands are aligned closely with island or seamounts with historic or Holocene eruptions and many are associated with sites of persistent hydrothermal activity (e.g. Hekinian *et al*. 2008; Kim *et al*. 2009; Siebert *et al*. 2010).

The detected acoustic signals show differing time-frequency characteristics, both between and within bands. Volcanoacoustic signals arise from a suite of physical processes that may include the subsurface magma movement, seafloor eruptions, degassing, earthquakes and landslide activity. In assessing unrest within the volcano, the paper considers only the rate of coherent acoustic activity, integrating signals associated with these various processes operating in the shallow crust or at the seafloor interface. This aggregate approach is similar to the use of seismic rms or heat flux as a proxy for unrest and triggered response in subaerial volcanoes (e.g. Harris & Ripepe 2007; Cannata *et al*. 2010; Delle Donne *et al*. 2010).

Fig. 7 shows a cumulative plot of the normalized number of detections arriving from various azimuth bands as a function of time. The cumulative count incorporates arrivals within 1.65 standard deviations from the band's mean (∼90 per cent confidence interval), as defined by a local fit to the histogram of detection azimuths

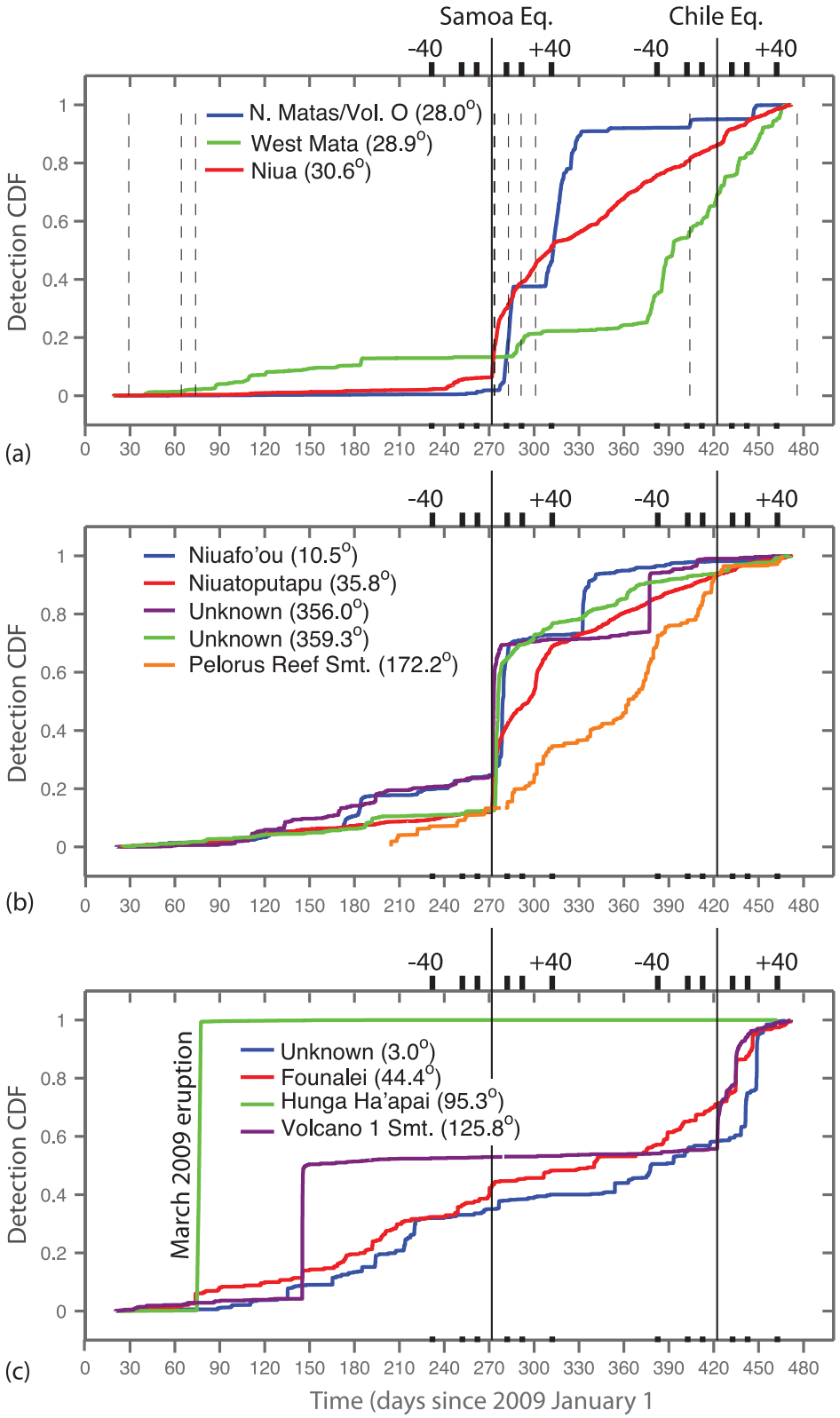

Figure 7. Cumulative distribution plots for the primary detection bands. Solid vertical lines show times of the 2009 Samoan and 2010 Chilean earthquakes. Bold tick marks delineate 10, 20 and 40 d windows on either side of these seismic events. (a) Azimuths associated with volcanic source near the Matas/Vol. O (28.00°), West Mata (28.93°) and the Niua vent field (30.62°). All three bands show an increase detection rate in the hours-to-weeks following the 2009 Samoan earthquake. Dashed vertical lines show other $M \geq 5.5$ earthquakes within 1° distance of West Mata. (b) Five other detection bands (10.53°, 35.80°, 171.89°, 355.99°, 359.29°) responding to 2009 Samoan earthquake with an increase in detection rate (c) Four detection bands (2.95°, 44.40°, 95.31°, 125.75°) not responding to the 2009 Samoan earthquake, three of which appear to respond following the 2010 Chilean earthquake.

(Fig. 3, Table 1). The two solid vertical lines in Fig. 7 mark the times of the great Samoan earthquake in 2009 September and the great Chilean earthquake in 2010 February.

For clarity, the 12 detection bands are distributed into three panels. Fig. 7(a) shows detections associated with the three sources located within the NE corner of the basin, West Mata Volcano (28.93°), the northern Matas/Volcano O caldera (28.00°) and Niua Volcano (30.62°). Each of these bands shows an increase in the rate of acoustic detections before and after the great Samoan earthquake, but no response to the Chilean earthquake. Fig. 7(b) shows the five other detection bands that respond positively to the Samoan earthquake, and have no response to the more distant Chilean earthquake. Fig. 7(c) shows the four persistent source bands that show no response to the Samoan earthquake; however, three of these sources show a rate increase in the time period following the great Chilean earthquake.

In the wake of the large regional Samoan earthquake, there was abundant aftershock activity both across the outer rise and within the overriding plate (Beavan *et al*. 2010; Lay *et al*. 2010). Aftershocks epicentres span a range of azimuths between 27° and 42°. In keeping with Omori's (1894) and Båth's (1965) Laws most of the teleseismically detected ($M > 4.5$) events occur in the first week after the main shock (Fig. 3). Somewhat surprisingly, increased levels of transient aftershock noise do not mask out the persistent source bands identified prior to the earthquake. Rather, these bands show an increased level of activity that is not observed at neighbouring azimuths that span the broader aftershock zone (Fig. 3b). This increase in activity also continues well beyond the time period of the most intense aftershock activity, and notably extends to azimuths distal to the aftershock zone (Figs 1 and 3).

The onset times of the detection rate increases vary from band-to-band. Fig. 8 shows an enlarged view of the cumulative count data (Fig. 7) spanning the 10- and 20-d periods before and after the great Samoan and Chilean earthquakes, respectively. For the bands responding to the Samoan earthquake, the 28.93°, 30.62° and 35.80° bands show a clear onset within 1–2 hr after the main shock. The remaining bands show increases that begin at approximately 0.7 d (355.99°), 1.0 d (10.53°), 1.7 d (359.29°) and 5 d (28.00°).

For those bands that appear to respond to the Chilean earthquake, the 125.75° band shows an increase in detection rate that begins ∼1.8 hr after the earthquake origin. This band had been quiet since the seismic swarm on 2009 May 26 (Fig. 8c). For the 44.40° azimuth band, the detection rate increases abruptly 12.45 d after the great Chilean earthquake. The timing of this detection increase is correlated with (lagging by only 30 min) a second swarm of detections associated with the 125.75° azimuth band. There are no large local earthquakes that might explain this correlation; curiously however, both increases occur less than 2 hr after a pair of large *M*s ∼7.1 Chilean aftershocks that occurred within 15 min of each other on 2010 March 11. Increases in detection rate within the 2.95° band occur even later, and are manifest by two swarms of detections beginning at 16 and 19 d after the great Chilean earthquake (Fig. 8c).

4.2 Quantifying detection rate changes

To determine if a change in detection rate is significant, we assume that the number of detections made during a given time window represents the outcome of a Poisson process. A doubling in the number of detections between time periods therefore does not necessarily mean the ensemble average rate increased by two. Instead

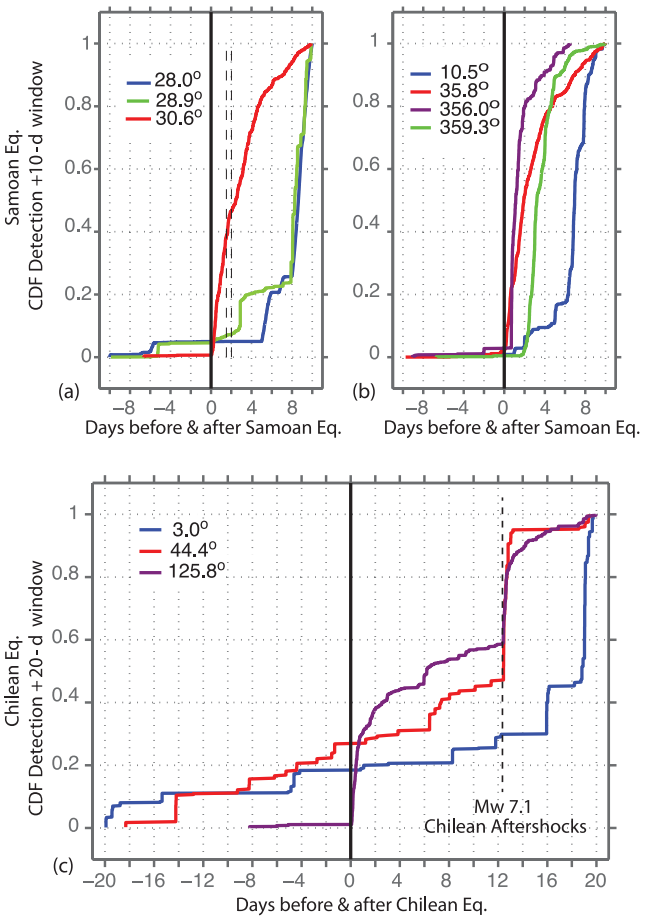

Figure 8. Cumulative distribution plots for the primary detection bands for 10- and 20-d windows surrounding the times of the Samoan and Chilean earthquakes, respectively. (a) Azimuths associated with volcanic source near West Mata, the Matas/Vol. O and the Niua vent field. Dashed vertical lines show other $M \geq 5.5$ earthquakes within 1° distance of West Mata (ISC 2011). (b) Detection bands 10.53°, 35.80°, 355.99° and 359.29°. Note that 171.89° band is excluded here due to air-gunning in the days immediately following the Samoan earthquake. (c) Detection bands that show a positive increase in detection rate following the 2010 Chilean earthquake.

the probability of such an instance being observed by chance must be assessed.

The probability density function (pdf) of the rate λ for N detections occurring during a period Δt is given as (Marsan & Nalbant 2005; Marsan & Wyss 2011):

$$f(\lambda) = \Delta t \mathrm{e}^{-\lambda \Delta t} \frac{(\lambda \Delta t)^N}{N!}. \quad (1)$$

The pdf of the rate before $f_b(\lambda_b)$ and after $f_a(\lambda_a)$ a given event can therefore be defined, and combined to estimate the probability that the rate increase exceeds a value r.

$$P\left(\frac{\lambda_a}{\lambda_b} > r\right) = \int_0^\infty \mathrm{d}\lambda_b f_b(\lambda_b) \int_{r\lambda_b}^\infty \mathrm{d}\lambda_a f_a(\lambda_a), \quad (2)$$

where the above expression is solved numerically (Marsan & Wyss 2011).

To illustrate these concepts, consider a simple example where 30 detections occur over a 10-d period, and then 50 detections are made during the next 10-d period ($N_a = 30$, $N_b = 50$, $\Delta t = 10$). The pdf of the rate function for each group is shown in Fig. 9(a), with maximum likelihood values of $\lambda_b = 30/10 = 3$ and $\lambda_a = 50/5 = 5$.

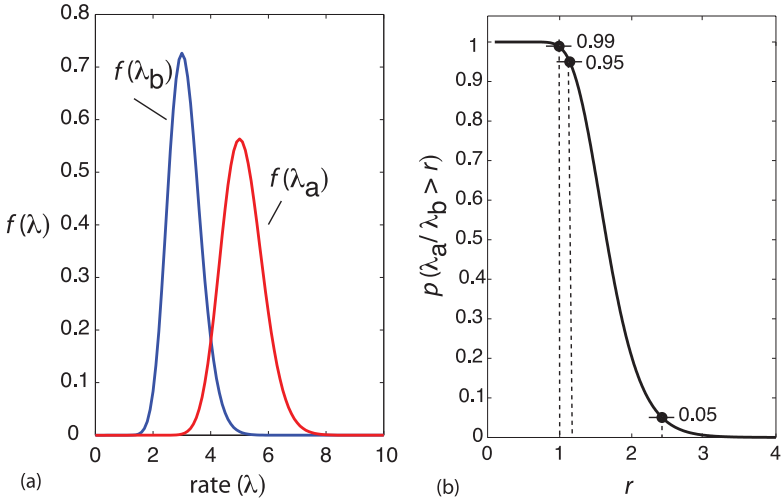

Figure 9. (a) Hypothetical probability density functions of the rate of acoustic detection (1 d^{-1}) observed in the 10 d before and 10 d after a great earthquake. (b) Probability of a change in detection rate greater than ratio r, given the observed rates. In this example, there is a >0.99 probability that rate increased ($r > 1$) after the great earthquake. The rate increase is constrained to lie between 1.14 and 2.42 with 90 per cent confidence. See Section 4.1 for additional description. Figure concept after Marsan & Wyss (2011).

This is nominally a 1.67-time increase in the rate; however, to assess the uncertainty eq. (2) is evaluated for a suite of r values. The result (Fig. 9b) shows that there is only a 1 per cent probability that the true rate did not show a positive increase (i.e. that r is less than 1) and defines the 90 per cent confidence interval for the rate change, $r_{90\text{ per cent}} = 1.14$–$2.42$.

For each of the 12 persistent detection bands, this procedure is used to quantify the rate change with respect to the two great earthquakes. The results for 2009 Samoan earthquake are given in Table 2. Four time periods are assessed. The change in detection rate in the time period extending from the start of the deployment through the main shock earthquake origin time ($\Delta t_b = 252.7$ d) is compared to the time period after the event ($\Delta t_a = 200.3$ d), and three different time windows of 10, 20 and 40 d ($\Delta t_b = \Delta t_a$) on either side of the main shock are assessed. These three windows span a range of reported repose times between seismic activity and triggered eruptions at other volcanoes and geysers (Manga & Brodsky 2006; Delle Donne *et al*. 2010). For the 125.75° and 171.89° bands, seismic air-gunning activity contaminates the record during the first 10-d window after the main shock. As such we evaluate only the long-term change in detection rate, which is assessed by simply muting out detections in these bands during the period of the seismic survey.

For the purposes of this study, rate changes $r_{90\text{ per cent}} > 2.0$ are considered significant and are highlighted in bold font in Table 2. Of the 12 bands, only four bands, at azimuths of 2.95°, 44.40° (Founalei Is.), 95.31° (Hunga Ha'apai) and 125.75°, fail to show a positive rate increase within each of the four time windows considered relative to the Samoan earthquake. The 171.89° azimuth band exhibits a significant ($r = 6.06$–10.26) rate increase over the largest time window, but smaller ($r_{90\text{ per cent}} < 2$) positive rate increases within the 20- and 40-d windows. For the remaining seven bands that respond to the Samoan earthquake, $r_{90\text{ per cent}}$ rate changes vary from ∼4 to 200 times over all four time windows. The largest rate increases are associated with azimuth bands centred at 10.53° (Niuafo'ou), 30.62° (Niua) and 359.29° over the initial 10 d, and 28.93° (West Mata volcano) over the 20-d window (Table 2).

None of the seven bands that show a response to the Samoan earthquake show a significant positive response to the Chilean earthquake, nor does the 95.31° band associated with Hunga Ha'apai (Fig. 7). Table 3 shows rate changes following the Chilean earthquake for the remaining three bands. Windows of 10, 20 and 40 d are assessed. The 125.75° azimuth band, associated with Volcano 1 seamount, shows a rate increase of at least 32 times within each of the time windows. The remaining two bands (2.95°, 44.40°) show a possible delayed response—with no significant increase over the initial 10-d window and small, but significant, increases over the 20- and 40-d windows. Notably, if these later rate increases do occur in response to Chilean earthquake, their onset is delayed by 1–2 weeks relative to what is observed following the Samoan earthquake (Fig. 7).

5 DISCUSSION AND CONCLUSIONS

5.1 Acoustic signatures of volcanic unrest

In all instances, the generation of underwater sound requires some mechanical source (e.g. Lighthill 1978). For submarine volcanoes, common sources include triggered seismicity in response to fluctuating magma pressure, the movement of fluids within the volcanic conduit, the expulsion of lava and gas at the seafloor interface and gravity-driven slope failure. The aggregated rate at which such processes occur is therefore a proxy for overall state of unrest within a volcanic system.

Although the use of T waves in studying submarine volcanoes is not new (e.g. Dietz & Sheehy 1954; Norris & Johnson 1969; Norris & Hart 1970; Talandier & Okal 1987), this work highlights the potential for short-base line sound-channel moored hydrophone arrays to monitor large sections of arcs and other submarine volcanic chains with great precision. Of the approximately 18 active volcanoes along the Tofua Arc (Siebert *et al*. 2010), six are identified as persistent noise sources, being acoustically active over a significant portion of the 15-month monitoring period. These include acoustic sources located on or near Niuafo'ou Is., the northern Matas/Vol. O, West Mata, Founalei Is., Hunga Ha'apai Is. and Volcano 1 seamount at 21°10′S, 175°45′W. Not surprisingly, those volcanoes with documented eruptions during the monitoring period (Hunga Ha'apai and West Mata) are among the most acoustically active (Vaughan & Webley 2010; Resing *et al*. 2011; Bohnenstiehl *et al*. 2013).

Table 3. Rate changes before and after the 2010 Chilean earthquake.

Az. band	$T_b = T_a = 10$ d		$T_b = T_a = 20$ d		$T_b = T_a = 40$ d	
Table key →	N_b / N_a	$r_{90\ per\ cent}$	N_b / N_a	$r_{90\ per\ cent}$	N_b / N_a	$r_{90\ per\ cent}$
2.95	58 / 45	0.76–1.26	131 / 555	**3.76–5.01**	268 / 1321	**4.51–5.51**
44.40	64 / 68	1.01–1.51	108 / 295	**2.51–3.51**	173 / 461	**2.51–3.26**
125.75	20 / 1061	**36.51–75.76**	20 / 1877	**64.5–133.8**	49 / 2020	**32.51–52.26**

Note: Bold values indicate positive rate changes with $r_{90\ per\ cent} > 2$.

Along the Tofua Arc, the detection data also identify persistent acoustic activity associated with an Pelorus Reef seamount near 22°50′S, 176°25′W, as well as sites within the Niua hydrothermal field and volcanic terrain to the south of Niuatoputapu Island (Figs 1 and 3). In the northern Lau Basin, three more bands of persistent activity are identified; however, seafloor and water column mapping are sparse within this region of the basin and the azimuthal constraints provided by the correlation detector are insufficient to uniquely associate these bands with specific edifices. Nonetheless, identification of these persistent volcanoacoustic noise sources—in areas without documented historical eruptions—suggests that the observational record (e.g. Siebert *et al*. 2010) may not provide a complete accounting of active submarine volcanic centres within the basin and arc. This likely reflects the fact that many submarine eruptions produce little or no evidence at the sea surface and few earthquakes of sufficient size to be detected at teleseismic distances.

Persistent acoustic activity focused towards Hunga Ha'apai was ongoing at the time monitoring began in 2009 January and continued through the eruption in 2009 March (Fig. 3a; Bohnenstiehl *et al*. 2013). Post eruption, the detection rate continued to decline as degassing and steam eruptions became less frequent. By midsummer 2009, the volcano entered a period of silence that continued through the end of the deployment in 2010 April (Fig. 3a). Bohnenstiehl *et al*. (2013) interpret the persistent precursory noise to track the build-up of stress within the system prior to the eruption, and the declining detection rates after the eruption therefore track the relaxation of stress, some component of which may be thermally driven.

Expanding this interpretative framework to the basin scale suggests that tracking low-level acoustic noise may provide a mechanism to assess the current hazard associated with submarine volcanoes. Notably many Tofua Arc volcanoes with documented eruptive activity in recent decades, such as Tofua Island (VEI 0–1 eruptions in 2004, 2006, 2008 and 2009), Metis Shoal (VEI 2 eruption in 1995) and Home Reef (VEI 2 eruption in 2006) (Siebert *et al*. 2010), do not show elevated rates of acoustic activity. This would suggest a lower short-term likelihood of eruptions at these sites; however, the timescale over which the system might transition to an acoustically active state and the implications of this change for eruption forecasting cannot be constrained from this single 15-month duration study.

5.2 Detection rate changes following great earthquakes

Interactions between strong earthquakes and volcanoes are now well documented in subaerial settings, where volcanic systems are monitored most commonly by a combination of remote sensing techniques and local seismometer arrays. Commonly reported responses include triggered seismicity and tremor (e.g. West *et al*. 2005), an increased frequency of eruption (e.g. Watt *et al*. 2009) and changes in the style or intensity of ongoing volcanic activity (e.g. Linde & Sacks 1998; Walter & Amelung 2007). These activities may be initiated in response to static stress changes, which represent a permanent deformation of the lithosphere in response to dislocation along the fault rupture plane, and/or by transient dynamic stresses associated with the passage of seismic waves. Static stresses fall of as $1/r^3$, where dynamic stresses fall of more gradually with range. For surface waves, for example, empirical observations show that amplitude decreases as $\sim 1/r^{1.66}$ (Lay & Wallace 1995). The radiation pattern, directivity of the rupture and crustal structure of course also influence the amplitude of ground shaking at any location (Manga & Brodsky 2006; Delle Donne *et al*. 2010).

Proposed mechanisms that might lead to heightened unrest at a volcano include compression (increasing reservoir pressure) and dilation (promoting tensile fracturing) of the magma chamber, nucleation of bubbles within the magma and the generation of landslides that can affect state of stress within shallow magma reservoirs. Passing seismic waves may also alter the permeability structure, resulting in the movement of hydrothermal fluids and changes in the effective stress along fault zones (generating earthquakes). The closing and opening of cracks within the conduit might also modulate the escape of gas through the volcanic carapace.

Along the submarine Tofua Arc, the response of volcanic systems is quantified by examining the rate of correlation-based detections as a function of azimuth. Importantly, this approach allows us to simultaneously assess the response of multiple volcanoes using a consistent metric. Of the 12 persistent acoustic source bands identified, seven show a positive response following an *M*w 8.1 earthquake that occurred on 2009 September 29; this outer rise normal faulting event spawned two nearly coseismic *M*w 7.8 thrusts along the Tongan Trench and a spatially distributed aftershock field that activated faults within the overriding plate (Beavan *et al*. 2010; Lay *et al*. 2010). Persistent acoustic source centred at 35.5° (Niuatoputapu Is.) 28.00, 28.93 and 30.62° (northern Matas/Vol. O, West Mata and Niua) azimuths are positioned only ∼180 km (∼1 rupture length) from the centroid of the *M*w 8.1 rupture. They are located well within the aftershock cloud (Fig. 4) and adjacent to the zone of thrust faulting, suggesting that magmatic systems within this region might be influenced principally by the static deformation of the overriding plate. The three other sources that show a positive response to the event lie at ranges of 400–900 km, where the amplitudes of dynamic stresses changes likely exceed static stress changes (Manga & Brodsky 2006).

Delle Donne *et al*. (2010) have summarized the distance–magnitude envelope for volcanic responses to large earthquakes,

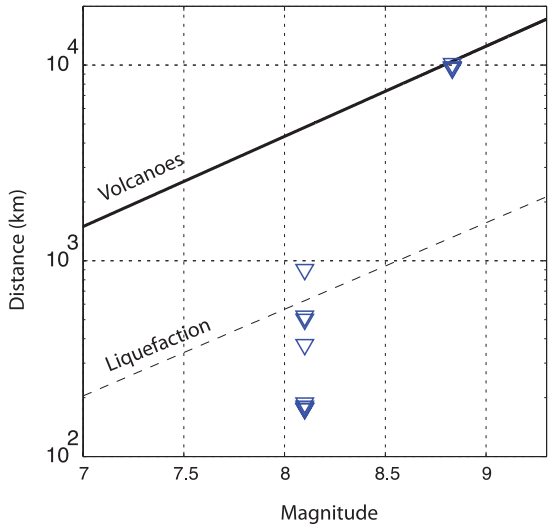

Figure 10. Plot of earthquake magnitude versus distance for volcanoes responding to the great Samoan and Chilean earthquakes. Solid line shows the relationship defined by Delle Donne *et al*. (2010) for volcanoes; $M = -6.4 + 2.17 \log_{10}(R)$. Dashed line shows relationship for earthquake-induced liquefaction in soils; $M = -5.0 + 2.26 \log_{10}(R)$ (Wang *et al*. 2005).

using data from a suite of observations around the globe (Bautista *et al*. 1996; Linde & Sacks 1998; Lara *et al*. 2004; Brodsky & Prejean 2005; Gresta *et al*. 2005; West *et al*. 2005; Cigolini *et al*. 2007; Walter *et al*. 2009). As illustrated in Fig. 10, submarine volcanoes throughout the Lau Basin and Tofua Arc all lie at ranges much less than the maximum expected response distance of ∼4800 km for an *M*w 8.1 earthquake. In this context, the response of these volcanoes is in no way unusual. Response initiation times range from a few hours to 5 d. These results also are in keeping with global observations of volcanic responses following previous great earthquakes (e.g. Linde & Sacks 1998; Delle Donne *et al*. 2010).

Of the four bands that did not show a response to the 2009 Samoan earthquake, one is Hunga Ha'apai, which erupted in 2009 March 2009 and entered a state of acoustic silence months before the Samoan earthquake. Another is the Volcano 1 seamount (21°10′S, 175°45′W), which underwent a short but intense swarm in 2009 May and then also became relatively silent in months thereafter. Certainly, in the case of a significant (VEI 2) eruption like that observed at Hunga Ha'apai, stress would have been relaxed and the gas expelled from the system during the eruption. This likely would desensitize the volcano to external dynamic shaking.

The Volcano 1 seamount, however, does respond months later to the great *M*w 8.8 Chilean event in 2010 February. The response is characterized by a series of low-frequency, long-duration sounds that begin within 1.8 hr of the event origin (Fig. 6). The onset time of the observed rate increase is therefore keeping with the delays seen at the other volcanic systems following the Samoan earthquake, and occurs sometime after the initial passage of surface waves (*R*1) at ∼40 min after the origin. The Founalei Island band then shows an increased rate of detection that begins 12 d after the event, and approximately a week later a rate increase is observed within the 2.95° band. Although these more delayed responses are small in magnitude and their timing makes for a more tenuous association, they are nonetheless the largest rate increase observed in these bands during the 15-month period of monitoring (Fig. 7). Empirical observations suggest that earthquakes as large as the 2010 Chilean event may produce a response from volcanoes as far away as $\sim 10^4$ km (i.e. globally; Fig. 10), and the Chilean earthquake previously has been shown to trigger microseismicity and tremor in southern California at ∼9300 km range (e.g. Peng *et al*. 2010). Consequently, the response of a few volcanoes within the Lau Basin and Tofua Arc to the Chilean earthquake would not be unexpected.

The results indicate that those submarine volcanic systems with an active acoustic state are sensitive to static and dynamic stress changes following great earthquakes. Notably, we do not see widespread awakening of volcanoes that were silent before the eruption. There is, however, arguably one new band of activity located at an azimuth of ∼25° (Fig. 3b) that was not observed to persist prior to the Samoan earthquake, but is evident in the weeks following. This azimuth is in line with the Northeast Lau Spreading Center (NELSC, Fig. 1), which has had at least two recent eruptions—one in 2008 ($z = 1650$ m) (Rubin *et al*. 2009; Baker *et al*. 2011) and one a few years (1996–2008) earlier that has been identified by bathymetric differencing (R. Embley, personal communication, 2013).

Those systems that responded to the Samoan earthquake in late 2009 September, do not respond to the Chilean earthquake 5 months later. This may reflect the fact that still elevated detection rates following the Samoan earthquake mask any response to the Chilean event, but it also could indicate that the response following the Samoan earthquake (degassing and stress relaxation) pushed these volcanic systems further from the critical state of stress where they are susceptible to such perturbations. Notably acoustic source regions responding to the Chilean event are positioned distant to the Samoan earthquake.

Gas eruption events in response to great earthquakes have been document through *in situ* monitoring at Stromboli and Etna Volcanoes (e.g. Cigolini *et al*. 2007; Walter *et al*. 2009) and in association with triggered eruptions at mud-volcanoes (Manga *et al*. 2009; Rudolph & Manga 2010). While short-term measurement of CO_2 flux estimates from submarine arc volcanoes suggest they play an import role in modulating CO_2 levels on geological timescales (e.g. Dziak *et al*. 2012), in such environments the importance of transient gas release events following great earthquakes likely can only be assessed with long-term *in situ* monitoring.

While these two great earthquakes are obvious targets for our investigations, large (*M*w > 6) earthquakes are not uncommon along the Tonga–Pacific plate boundary. During the period of this monitoring experiment, however, only one such event occurred along the shallow subduction interface in the vicinity of the array (excluding those associated with the 2009 Samoan earthquake). This event (*M* 7.6) on March 19 ruptured a section of the plate boundary to the south of Tongatapu Island, with a hypocentre positioned at 23.050°S 174.668°W and at a depth of 34 km (Fig. 1). It occurred less than a day after the succession of surtseyan (VEI 2) eruptions on Hunga Ha'apai, but did not reinvigorate its eruptive activity. It also does not appear to have trigger a response at other volcanoes along the arc, although it is possible that small acoustic events may have been masked by elevated underwater noise associated with waning volcanic activity and stream eruptions at Hunga Ha'apai.

6 CONCLUSIONS

Correlation-based acoustic detectors provide a metric through which to simultaneously monitor volcanic unrest across large sections of the Tofua Arc and Lau Basin. During the 15-month monitoring period, 12 persistent acoustic sources are identified within the ambient underwater sound field. Most of these detection bands align with submarine volcanic features, including sites of known

eruptive activity associated with West Mata and Hunga Ha'apai volcanoes. Observations following the 2009 Samoan (*M*w 8.1) and 2010 Chilean earthquakes indicate that acoustically active submarine volcanoes may lie in a critical state of unrest that makes them susceptible to the accompanying static and dynamic stress changes. Submarine volcanoes respond in a similar fashion to those on land, with signs of unrest initiated within hours to days of the triggering earthquake at ranges consistent with the scaling defined by Delle Donne *et al.* (2010). Great earthquakes may have undocumented impacts on Earth's vast submarine volcanic systems, and may even serve to modulate the transient flux of magma and volcanic gas into the overlying ocean.

ACKNOWLEDGEMENTS

We thank the captain and crew of the R/V Marcus G. Langseth, R/V Roger Revelle and R/V Kilo Moana. Critical to the success of this project were the National Oceanic and Atmospheric Administration (NOAA) field technicians J. Shanley and M. Fowler, who oversaw the mooring deployment and recovery efforts, and the North Carolina State University (NCSU) graduate students J. Bowman, K. Cook, P. Monigle, J. O'Connor, C. Scheip and K. Warren. F. Martinez kindly provided his Lau Basin bathymetry compilation (Fig. 1). R. Embley generously reviewed and early draft of this manuscript. We are grateful for input from an anonymous reviewer, who helped to identify additional information on Volcano 1 and Pelorus Reef seamounts. This is NOAA-PMEL contribution #4012. The work was supported by National Science Foundation grants OCE-0825295 and OCE-1029278.

REFERENCES

Baker, E.T., Lupton, J.E., Resing, J.A., Baumberger, T., Lilley, M.D., Walker, S.L. & Rubin, K.H., 2011. Unique event plumes from a 2008 eruption on the Northeast Lau Spreading Center, *Geochem. Geophys. Geosyst.,* **12,** Q0AF02, doi:10.1029/2011GC003725.

Bautista, B.C. *et al.*, 1996. Relationship of regional and local structures to Mount Pinatubo activity, in *Fire and Mud: Eruptions and Lahars of Mount Pinatubo, Philippines,* pp. 351–370, eds Newhall, C.G. & Punongbayan, R.S. *et al.*, University of Washington Press.

Båth, M., 1965. Lateral inhomogeneities in the upper mantle, *Tectonophysics,* **2,** 483–514.

Beavan, J., Wang, X., Holden, C., Wilson, K., Power, W., Prasetya, G., Bevis, M. & Kautoke, R., 2010. Near-simultaneous great earthquakes at Tongan megathrust and outer rise in September 2009, *Nature,* **466,** 959–963.

Bevis, M. *et al.*, 1995. Geodetic observations of very rapid convergence and back-arc extension at the Tonga arc, *Nature,* **374,** 249–251.

Bohnenstiehl, D.R., Scheip, C., Matsumoto, H. & Dziak, R.P., 2012. Acoustic variability of airgun signals recorded at intermediate ranges within the Lau Basin, *Geochem. Geophys. Geosyst.,* **13,** doi:10.1029/2012GC004337.

Bohnenstiehl, D.R., Dziak, R.P., Matsumoto, H. & Lau, T.K., 2013. Underwater acoustic records from the March 2009 eruption of Hunga Ha'apai–Hunga Tonga volcano in the Kingdom of Tonga, *J. Volc. Geotherm. Res.,* **249,** 12–24.

Brodie, D. & Dunn, R., 2011. Detection of baleen whales on an ocean-bottom seismometer array in the Lau Basin, Abstract S31D-2266, *presented at 2011 Fall Meeting,* 5–9 December, AGU, San Francisco, California.

Brodsky, E.E. & Prejean, S.G., 2005. New constraints on mechanisms of remotely triggered seismicity at Long Valley Caldera, *J. geophys. Res.,* **110,** B04302, doi:10.1029/2004JB003211.

Cannata, A., Di Grazia, G., Montalto, P., Aliotta, M., Patanè, D. & Boschi, E., 2010. Response of Mount Etna to dynamic stresses from distant earthquakes, *J. geophys. Res.,* **115,** B12304, doi:10.1029/2010JB007487.

Chadwick, W.W. Jr., Wright, I.C., Schwarz-Schampera, U., Hyvernaud, O., Reymond, D. & de Ronde, C.E.J., 2008. Cyclic eruptions and sector collapses at Monowai submarine volcano, Kermadec arc: 1998–2007, *Geochem. Geophys. Geosyst.,* **9,** Q10014, doi:10.1029/2008GC002113.

Chadwick, W.W. Jr., Dziak, R.P., Haxel, J.H., Embley, R.W. & Matsumoto, H., 2012. Submarine landslide triggered by volcanic eruption recorded by in situ hydrophone, *Geology,* **40,** 51–54.

Chapp, E., Bohnenstiehl, D.R. & Tolstoy, M., 2005. Sound-channel observations of ice-generated tremor in the Indian Ocean, *Geochem. Geophys. Geosyst.,* **6,** Q06003, doi:10.1029/2004GC000889.

Cigolini, C., Laiolo, M. & Coppola, D., 2007. Earthquake-volcano interactions detected from radon degassing at Stromboli (Italy), *Earth planet. Sci. Lett.,* **257,** 511–525.

Conder, J.A. & Wiens, D.A., 2011. Shallow seismicity and tectonics of the central and northern Lau Basin, *Earth planet. Sci. Lett.,* **304,** 538–546.

Del Pezzo, E. & Giudicepietro, F., 2002. Plane-wave fitting method for a plane, small aperture, short period seismic array: a MATHCAD program, *Comput. Geosci.,* **28,** 59–64.

Delle Donne, D., Harris, A.J.L., Ripepe, M. & Wright, R., 2010. Earthquake-induced thermal anomalies at active volcanoes, *Geology,* **38,** 771–774.

Dietz, R.S. & Sheehy, M.J., 1954. Transpacific detection of Myojin volcanic explosions by underwater sound, *Bull. geol. Soc. Am.,* **65,** 941–956.

Dunn, R.A. & Martinez, F., 2010. Contrasting crustal production and rapid mantle transitions beneath back-arc ridges, *Nature,* **46,** 198–202.

Dunn, R.A., Martinez, F. & Conder, J.A., 2013. Crustal construction and magma chamber properties along the Eastern Lau Spreading Center, *Earth planet. Sci. Lett.,* **371–372,** 112–124.

Dziak, R.P. & Johnson, H.P., 2002. Stirring the oceanic incubator, *Science,* **296,** 1406–1407.

Dziak, R.P., Chadwick, W.W., Fox, C.G. & Embley, R.W., 2003. Hydrothermal temperature changes at the southern Juan de Fuca Ridge associated with *M*w 6.2 Blanco Transform earthquake, *Geology,* **31,** 119–122.

Dziak, R.P., Haxel, J.H., Matsumoto, H., Lau, T.K., Merle, S.G., de Ronde, C.E.J., Embley, R.W. & Mellinger, D.K., 2008. Observations of regional seismicity and local harmonic tremor at Brothers volcano, south Kermadec arc, using an ocean bottom hydrophone array, *J. geophys. Res.,* **113,** B08S04, doi:10.1029/2007JB005533.

Dziak, R.P., Baker, E.T., Shaw, A.M., Bohnenstiehl, D.R., Chadwick, W., Haxel, J.H., Matsumoto, H. & Walker, S.L., 2012. Flux measurements of explosive degassing using a yearlong hydroacoustic record at an erupting submarine volcano, *Geochem. Geophys. Geosyst.,* **13,** Q0AF07, doi:10.1029/2012GC004211.

Eguchi, T., Fujinawa, Y. & Ukawa, M., 1989. Microearthquakes and tectonics in an active back-arc basin: the Lau Basin, *Phys. Earth planet. Inter.,* **56,** 210–229.

Embley, R.W. *et al.*, 2006. Long-term eruptive activity at a submarine arc volcano, *Nature,* **441,** 494–497.

Fox, C.G., Matsumoto, H. & Lau, T.-K.A., 2001. Monitoring Pacific Ocean seismicity from an autonomous hydrophone array, *J. geophys. Res.,* **106,** 4183–4206.

Gresta, S., Ghisetti, F., Privitera, E. & Bonanno, A., 2005. Coupling of eruptions and earthquakes at Mt. Etna (Sicily, Italy): a case study from the 1981 and 2001 events, *Geophys. Res. Lett.,* **32,** doi:10.1029/2004GL021479.

Harris, A.J.L. & Ripepe, M., 2007. Regional earthquake as a trigger for enhanced volcanic activity: evidence from MODIS thermal data, *Geophys. Res. Lett.,* **34,** L02304, doi:10.1029/2006GL028251.

Hekinian, R., Mühe, R., Worthington, T.J. & Stoffers, P., 2008. Geology of a submarine volcanic caldera in the Tonga Arc: dive results, *J. Volc. Geotherm. Res.,* **176,** 571–582.

International Seismological Centre (ISC), 2011. *On-line Bulletin,* Internatl. Seis. Cent., Thatcham, United Kingdom. Available at: http://www.isc.ac.uk, last accessed 21 June 2013.

Johnson, H.P., Dziak, R.P., Fisher, C.R., Fox, C.G. & Pruis, M.J., 2001. Earthquakes influence distant hydrothermal vents: the far-field effect and delayed response, *EOS, Trans. Am. geophys. Un.,* **82,** 233–236.

Johnson, R.H., Norris, R.A. & Duennebier, F.K., 1968. Abyssally generated *T*-phases, in *The Crust and Upper Mantle of the Pacific Area,* pp. 70–78,

eds Knopoff, L., Drake, C.L. & Hart, P.J., Geophysics Monograph, 12, American Geophysics Union.

Kim, H.-J. *et al.*, 2013. Caldera structure of submarine Volcano #1 on the Tonga Arc at 21°09′S, southwestern Pacific: analysis of multichannel seismic profiling, *Earth Planets Space,* **65,** 893–900.

Kim, J., Son, S.-K., Son, J.-W., Kim, K.-H., Shim, W.J., Kim, C.H. & Lee, K.-Y., 2009. Venting sites along the Fonualei and Northeast Lau Spreading Centers and evidence of hydrothermal activity at an off-axis caldera in the northeastern Lau Basin, *Geochem. J.,* **43,** 1–13.

Lara, L.E., Naranjo, J.A. & Moreno, H., 2004. Rhyodacitic fissure eruption in Southern Andes (Cordon Caulle; 40.5°S) after the 1960 (Mw: 9.5) Chilean earthquake: a structural interpretation, *J. Volc. Geotherm. Res.,* **138,** 127–138.

Lay, T. & Wallace, T.C., 1995. *Modern Global Seismology,* Academic Press.

Lay, T., Ammon, C.J., Kanamori, H., Rivera, L., Koper, K.D. & Hutko, A.R., 2010. The 2009 Samoa-Tonga great earthquake triggered doublet, *Nature,* **466,** 964–968.

Lighthill, M.J., 1978. *Waves in Fluids,* Cambridge Univ. Press.

Linde, A.T. & Sacks, I.S., 1998. Triggering of volcanic eruptions, *Nature,* **395,** 888–890.

Manga, M. & Brodsky, E., 2006. Seismic triggering of eruptions in the far field: volcanoes and geysers, *Annu. Rev. Earth planet. Sci.,* **34,** 263–291.

Manga, M., Brumm, M. & Rudolph, M.L., 2009. Earthquake triggering of mud volcanoes, *Mar. Pet. Geol.,* **26**(9), 1785–1798.

Marsan, D. & Nalbant, S.S., 2005. Methods for measuring seismicity rate changes: a review and a study of how the Mw 7.3 Landers earthquake affected the aftershock sequence of the Mw 6.1 Joshua Tree earthquake, *Pageoph,* **162,** 1151–1185.

Marsan, D. & Wyss, M., 2011. Seismicity rate changes, *Community Online Resource for Statistical Seismicity Analysis,* doi:10.5078/corssa-25837590, Available at: http://www.corssa.org, last accessed 21 June 2013.

Matsumoto, H., Haxel, J.H., Dziak, R.P., Bohnenstiehl, D.R. & Embley, R.W., 2011. Mapping the sound field of an erupting submarine volcano using an acoustic glider, *J. acoust. Soc. Am.,* **129,** EL94–99.

Nautilus Minerals Inc., 2008. NAT004 Nautilus Exploration Report: Papua New Guinea, Tonga, Fiji, Solomon Islands and New Zealand. Available at: http://www.nautilusminerals.com/i/pdf/2008NautilusExplorationNI43-101Report.pdf, last accessed 21 June 2013.

National Oceanographic and Atmospheric Administration, 2012. Ring of Fire Cruise narrative. Available at: http://oceanexplorer.noaa.gov/explorations/12fire/logs/updates/media/niua_divesites.html, last accessed 21 June 2013.

Norris, R.A. & Hart, D.N., 1970. Confirmation of Sofar-hydrophone detection of submarine eruptions, *J. geophys. Res.,* **75,** 2144–2147.

Norris, R.A. & Johnson, R.H., 1969. Submarine volcanic eruptions recently located in the Pacific by SOFAR hydrophones, *J. geophys. Res.,* **74,** 650–664.

Omori, F., 1894. On the aftershocks of earthquakes, *J. Coll. Sci. Imperial Univ. Tokyo,* **7,** 111–200.

Peng, Z., Hill, D.P., Shelly, D.R. & Aiken, C., 2010. Remotely triggered microearthquakes and tremor in central California following the 2010 Mw8.8 Chile earthquake, *Geophys. Res. Lett.,* **37,** doi:10.1029/2010GL045462.

Resing, J.A. *et al.*, 2011. Active submarine eruption of boninite in the northeastern Lau Basin, *Nature Geosci.,* **4,** 799–806.

Richards, J.J, 1962. *Catalogue of the Active Volcanoes of the World, Part 8. Kermadec, Tonga, and Samoa*. International Association of Volcanology. 38 pp.

Rubin, K.H., Embley, R.W., Clague, D.A., Resing, J., Michael, P.J., Keller, N.S. & Baker, E.T., 2009. Lavas from active boninite and very recent basalt eruptions at two submarine NE Lau Basin sites, *EOS. Trans. Am. geophys. Un.,* **90** [*Fall Meeting Suppl.*, Abstract # V43I-05].

Rudolph, M.L. & Manga, M., 2010. Mud volcano response to the 4 April 2010 El Mayor-Cucapah earthquake, *J. geophys. Res.,* **115,** doi:10.1029/2010JB007737.

Schaff, D.P., 2008. Semiempirical statistics of correlation-detector performance, *Bull. seism. Soc. Am.,* **98,** 1495–1507.

Schreiner, A.E., Fox, C.G. & Dziak, R.P., 1995. Spectra and magnitudes of T-waves from the 1993 earthquake swarm on the Juan de Fuca Ridge, *Geophys. Res. Lett.,* **22,** 139–142.

Siebert, L., Simkin, T. & Kimberly, P., 2010. *Volcanoes of the World: An Illustrated Catalog of Holocene Volcanoes and Their Eruptions,* Smithsonian Institution Global Volcanism Program Digital Information Series GVP-3. Available at: http://www.volcano.si.edu/world/, last accessed 21 June 2013.

Slack, P.D., Fox, C.G. & Dziak, R.P., 1999. P wave detection thresholds, Pn velocity estimates, and T wave location uncertainty from oceanic hydrophones, *J. geophys. Res.,* **104,** 13 061–13 072.

Stoffers, P. *et al.*, 2003. Cruise Report SONNE 167, Louisville Suva–Wellington 12 Oct.–02 Dec. 2002: Kiel (*Univ. Kiel, Inst. Geowiss.*).

Stoffers, P. *et al.*, 2006. Submarine volcanoes and high-temperature hydrothermal venting on the Tonga arc, southwest Pacific, *Geology,* **34,** 453, doi:10.1130/G22227.1.

Talandier, J. & Okal, E.A., 1987. Seismic detection of underwater volcanism: the example of French Polynesia, *Pageoph,* **125,** 919–950.

Taylor, B., Zellmer, K., Martinez, F. & Goodliffe, A., 1996. Sea-floor spreading in the Lau back-arc basin, *Earth planet Sci. Lett.,* **144,** 35–40.

Taylor, P.W., 2003. Pumice sightings in the northern Tongan Region, October 2002. Australian Volcanological Investigations (AVI), Occasional Report No. 03/04.

Vaughan, R.G. & Webley, P.W., 2010. Satellite observations of a surtseyan eruption: Hunga Ha'apai, Tonga, *J. Volc. Geotherm. Res.,* **198,** 177–186.

Walter, T.R. & Amelung, F., 2007. Volcanic eruptions following M 9 megathrust earthquakes: implications for the Sumatra-Andaman volcanoes, *Geology,* **35,** 539–542.

Walter, T.R., Wang, R., Acocella, V., Neri, M., Grosser, H. & Zschau, J., 2009. Simultaneous magma and gas eruptions at three volcanoes in southern Italy. An earthquake trigger? *Geology,* **37,** 251–254.

Wang, C.Y., Manga, M. & Wong, A., 2005. Floods on Mars released from groundwater by impact, *Icarus,* **175,** 551–555.

Watt, S.F.L., Pyle, D.M. & Mather, T.A., 2009. The influence of great earthquakes on volcanic eruption rate along the Chilean subduction zone, *Earth planet. Sci. Lett.,* **277,** 399–407.

Watts, A.B. *et al.*, 2012. Rapid rates of growth and collapse of Monowai submarine volcano in the Kermadec Arc, *Nature Geosci.,* **5,** 1–6.

West, M., Sanchez, J.J. & McNutt, S.R., 2005. Periodically triggered seismicity at Mount Wrangell, Alaska, after the Sumatra earthquake, *Science,* **308,** 1144–1146.

Wright, I.C. *et al.*, 2008. Collapse and reconstruction of Monowai submarine volcano, Kermadec arc, 1998–2004, *J. geophys. Res.,* **113,** 1–13.

Yang, Y. & Forsyth, D.W., 2003. Improving epicentral and magnitude estimation of earthquakes from T phases by considering the excitation function, *Bull. seism. Soc. Am.,* **93,** 2106–2122.

Zellmer, K. & Taylor, B., 2001. A three-plate kinematic model for Lau Basin opening, *Geochem. Geophys. Geosyst.,* **2,** doi:10.1029/2000GC000106.